Carsten Gundlach, Ian Hawke and Stephanie J Erickson

E-mail: cjg@soton.ac.uk
School of Mathematics, University of Southampton, Southampton SO17 1BJ, UK

A conservation law formulation of nonlinear elasticity in general relativity

Abstract.

We present a practical framework for ideal hyperelasticity in numerical relativity. For this purpose, we recast the formalism of Carter and Quintana as a set of Eulerian conservation laws in an arbitrary 3+1 split of spacetime. The resulting equations are presented as an extension of the standard Valencia formalism for a perfect fluid, with additional terms in the stress-energy tensor, plus a set of kinematic conservation laws that evolve a configuration gradient ${\psi^A}_i$. We prove that the equations can be made symmetric hyperbolic by suitable constraint additions, at least in a neighbourhood of the unsheared state. We discuss the Newtonian limit of our formalism and its relation to a second formalism also used in Newtonian elasticity. We validate our framework by numerically solving a set of Riemann problems in Minkowski spacetime, as well as Newtonian ones from the literature.

1. Introduction

Neutron stars are believed to form a crystalline outer crust as they age and cool, but retain a fluid (probably superfluid) core [1]. A mathematical framework for weak solutions of general relativistic elasticity is likely to be indispensable for the modelling of neutron star crusts in at least two scenarios: starquakes and binary mergers.

Pulsars are observed to spin down at a regular rate, losing angular momentum through gravitational and/or electromagnetic radiation. Occasionally the rotation spins up suddenly. One model suggests that such a "glitch" occurs when the elastic crust breaks and the inertial moment of the star decreases suddenly as a consequence (e.g. [2]). It has also been suggested [3] that starquakes are the cause of soft gamma repeaters (SGRs). Quasi-periodic oscillations in the tails of giant flares in SGRs have been suggested [4] to provide direct observational evidence for crust oscillation modes, although the modelling of neutron star oscillations even in perturbation theory is complicated by the coupling between the crust, the fluid core and a strong magnetic field (see e.g. [5]). A correct model would of course have to be nonlinear. Finally we note that strong shocks also arise when two old neutron stars in a binary system merge. The detailed dynamics and features, such as the breaking strain (see [6]), of the crust, will determine when and where the crust breaks. This will in turn impact on the post-merger dynamics, such as the time taken by the remnant to collapse to a black hole (see e.g. [7]).

For all these scenarios, models must therefore comprise an elastic crust, a fluid core, and a magnetic field permeating both. As a step towards such models, we present here a formulation of (hyper)elastic matter in general relativity in the form of conservation laws amenable to solution by high-resolution shock-capturing (HRSC) numerical methods. These conservation laws are the union of the usual stress-energy conservation (dynamics), and a set of conservation laws for a deformation tensor (kinematics).

The kinematic equations are essentially the same in Newtonian and relativistic physics, but the literature on weak solutions of Newtonian elasticity uses Cartesian tensor notation, which obscures the geometric nature of the theory. In Sec. 2, we derive these equations carefully, using the language of differential geometry. Following Carter and Quintana [8], we begin with a map from spacetime to a 3-dimensional matter space. The main object we calculate with is its derivative $\psi^A{}_i$. As a partial derivative, this is subject to integrability conditions. Under a 3+1 split these become evolution equations and constraints, of a purely kinematic nature, both of which can be written as conservation laws. We show that their physical significance is to allow discontinuities in the density and kinks, but to forbid discontinuities in the crystal axes and the particle world lines.

The other, dynamical, half of the problem consists in finding the stress-energy tensor from $\psi^A{}_i$ and an equation of state. We do this in Sec. 3, following Karlovini and Samuelsson [9]. In particular, demanding covariance on both spacetime and matter space restricts the possible dynamics. The equation of state can relate only quantities that transform as scalars on both spacetime and matter space. For an ideal liquid, there are three of these, which can be taken to be the number density, internal energy, and entropy. In an ideal solid that is intrinsically isotropic (for example by averaging over randomly oriented microscopic crystal domains, or for a cubic lattice), there are precisely two additional scalars that characterise its (nonlinear) shear. Hence in addition to the pressure (the derivative of the energy with respect to volume),

the stress-energy tensor of an isotropic solid depends on two generalised forces (the derivative of the energy with respect to the two shear invariants).

In Sec. 4, we prove that our kinematic and dynamical equations together form a first-order system of evolution equations that, by constraint addition, can be made hyperbolic *if the constraints (12) are obeyed or not.* This property is crucial for the stability of numerical solutions in which the constraints are left to evolve freely, and hence finite difference error generically generates constraint violations. We use the methods of Beig and Schmidt [10], who proved symmetric hyperbolicity of an inequivalent first-order system (one which would not be appropriate for modelling weak solutions).

In order to make contact with existing work on ideal fluid dynamics and magnetohydrodynamics in general relativity, in Sec. 5 we present our dynamical equations as a generalisation of the Valencia [11] formulation of hydrodynamics. We give an algorithm for the conversion between conserved and primitive variables.

As a first test of our formalism, in Sec 6 we present numerical time evolutions of Riemann problems and their equivalent in cylindrical symmetry, rotor problems. The variables are three-dimensional, and the grid is either one-dimensional, using the symmetry, or two-dimensional in either Cartesian or cylindrical coordinates, hiding the symmetry. We compare the relativistic code in the Newtonian limit with an explicitly Newtonian code, and both with published Newtonian Riemann problems [13, 12]. We also compare against exact Riemann solutions in the relativistic regime in Minkowski spacetime. We compare the Eulerian and mixed formalisms, and evolutions where the number density is either read off from the deformation tensor, or evolved separately.

In Sec. 7 we summarize the results of the paper, and discuss the work remaining to apply these methods to full 3+1 nonlinear simulations.

We collect relevant formulas from the standard 3+1 split of spacetime in Appendix A, and relevant definitions of hyperbolicity in Appendix B. One of two existing Newtonian formalisms [15, 14] is essentially the Newtonian limit of our formalism. We derive the Newtonian limit in Appendix C. In Appendix D we derive the equations of an alternative Newtonian formalism [16, 17, 18], and prove that the two have the same weak solutions. (This seems to be assumed in the literature, but is nontrivial.)

The remaining Appendices contain auxiliary material on our numerical method and our numerical tests: Appendix E proposes a general framework for discrete constraint preservation (similar to "constrained transport" for MHD). Appendix F presents our implementation of Riemann tests on a 2-dimensional Cartesian grid, and Appendix G our implementation of cylindrical coordinates. Appendix H reviews the freedom to choose two shear invariants, and Appendix I describes the equations of state we use. Appendix J summarizes how we construct exact solutions for specific Riemann problems and Appendix K the initial data for our Riemann tests used here.

We have attempted as far as possible to achieve compatibility with the notation of [9], [10] and [11]. Throughout this paper, tensor indices are assumed to be in a generic local *coordinate* basis. Partial derivatives in this basis are indicated by commas. Indices $a, b, c, \ldots = 0, 1, 2, 3$ are spacetime indices, $i, j, k, \ldots = 1, 2, 3$ are spatial indices on $x^0 = t =$ const. hypersurfaces, and $A, B, C, \ldots = 1, 2, 3$ are matter space indices on a 3-dimensional matter space X_3. In Appendix D (only), the indices $\alpha, \beta, \gamma, \ldots = 0, 1, 2, 3$ are matter space indices on an extended matter space X_4. In Secs. 3 and 4, $\alpha, \beta = 1, 2$ are used to label elastic forces. In Appendix B, $\alpha, \beta = 1, \ldots, n$ label the variables of a generic hyperbolic system. For all these indices a summation convention applies.

In order to take determinants of 2-index objects which are not (1,1) tensors, we introduce the non-tensorial totally antisymmetric symbol δ, which is defined to be $\delta_{0123} = 1$, etc. With the exception of the objects δ, throughout this paper, all objects transform as tensors of the type indicated by their free indices, unless we indicate otherwise by a suffix: for example, the determinant of the spacetime metric in coordinates x^a will be denoted by $-g_x$.

2. Kinematics

2.1. The configuration gradient and its 3+1 split

In the relativistic framework of [8, 9], the matter configuration is encoded in a map from 4-dimensional spacetime to 3-dimensional matter space

$$\chi : \quad M_4 \to X_3, \tag{1}$$

or in local coordinates x^a on spacetime and ξ^A on matter space,

$$x^a \mapsto \xi^A = \chi^A(x^a). \tag{2}$$

For simplicity of notation we denote the derivative $d\chi$ of χ by a new symbol ψ,

$$\psi : M_4 \to TX_3 \otimes T^*M_4, \tag{3}$$

$$x^a \qquad \mapsto \psi^A{}_a := \frac{\partial \xi^A}{\partial x^a}. \tag{4}$$

For time evolutions, we introduce a time-foliation of the spacetime, so that we have

$$\chi : R \times M_3 \to X_3, \tag{5}$$

$$(t, x^i) \qquad \mapsto \xi^A \tag{6}$$

with derivatives

$$\psi^A{}_i := \frac{\partial \xi^A}{\partial x^i}, \qquad \psi^A{}_t := \frac{\partial \xi^A}{\partial t}. \tag{7}$$

Following [19], we shall call χ^A the *configuration* and both $\psi^A{}_a$ and $\psi^A{}_i$ the *configuration gradient*.

The matter space coordinates ξ^A label particles and must therefore be constant along particle world lines, so that

$$u^a \psi^A{}_a = 0, \tag{8}$$

where the 4-velocity u^a is tangential to the matter world lines. Parameterising the 4-velocity in the standard way as

$$u^a = (u^t, u^i) = \alpha^{-1} W (1, \hat{v}^i) \tag{9}$$

(where α is the lapse, W the Lorentz factor and $\hat{v}^i$ a pseudo-Newtonian 3-velocity, see Appendix A for more details), we have

$$\psi^A{}_t = -\hat{v}^i \psi^A{}_i. \tag{10}$$

The configuration gradient $\psi^A{}_i$ is also used as the primary variable in the Newtonian framework of [15, 14, 21] (denoted there by g). This framework is the Newtonian limit of our relativistic one. In Appendix C we derive the Newtonian limit of our framework. Other Newtonian papers [18, 17] use the the 3×3 matrix inverse of $\psi^A{}_i$, which we shall denote by $F^i{}_A$, as the primary variable (denoted there by F).

We review this alternative framework in Appendix D. In the Newtonian literature, ${F^i}_A$ is commonly called the (Lagrangian) deformation gradient, and ${\psi^A}_i$ the inverse deformation gradient. From a geometric point of view, however, these objects on their own carry no information about what one might intuitively call a deformation.

2.2. Kinematic equations and hyperbolicity fix

From the definition of ${\psi^A}_a$ as a partial derivative, we have the integrability conditions

$$C^A{}_{ab} := \psi^A{}_{[a,b]} = 0. \tag{11}$$

In a 3+1 split, these become

$$C^A{}_{ij} := \psi^A{}_{[i,j]} = 0, \tag{12}$$

$$E^A{}_i \ := 2C^A{}_{it} = \psi^A{}_{i,t} + \left(\hat{v}^j \psi^A{}_j\right)_{,i} = 0. \tag{13}$$

The constraints (12) are conserved by the evolution equations (13). Note that these equations are already in conservation law form: more explicitly,

$$C^A{}_{ij} = \left(\psi^A{}_k \delta^k_{[i}\delta^l_{j]}\right)_{,l} = 0, \tag{14}$$

$$E^A{}_i \ = \psi^A{}_{i,t} + \left(\hat{v}^j \psi^A{}_j \delta^k_i\right)_{,k} = 0. \tag{15}$$

Instead of $E^A{}_i = 0$ as an evolution equation for ${\psi^A}_i$, we shall in fact use

$$\bar{E}^A{}_i := 2\alpha W^{-1} u^a C^A{}_{ia} = 2\psi^A{}_{[i,t]} + 2\hat{v}^j \psi^A{}_{[i,j]} = 0. \tag{16}$$

This can be written as a balance law obtained from the conservation law (13) by adding a source term that is proportional to the constraint (12), namely

$$\psi^A{}_{i,t} + \left(\hat{v}^j \psi^A{}_j\right)_{,i} = 2\hat{v}^j \psi^A{}_{[j,i]}. \tag{17}$$

Note that this cannot be written in pure conservation law form.

In handwaving anticipation of the hyperbolicity analysis presented in Sec. 4, we point out in passing that (17) can be written as an advection equation for ${\psi^A}_i$ with a source term that is of lower order in ${\psi^A}_i$, namely

$$\psi^A{}_{i,t} + \hat{v}^j \psi^A{}_{i,j} = -\psi^A{}_j \hat{v}^j{}_{,i}. \tag{18}$$

For *given* $\hat{v}^i$, this is strongly hyperbolic in ${\psi^A}_i$, whereas (13) is only weakly hyperbolic.

2.3. Kinematic jump conditions

As is well-known, different forms of balance laws that are equivalent for differentiable solutions can be inequivalent for weak solutions in the sense that they give rise to different Rankine-Hugoniot conditions. Therefore, it is important to derive the weak form of the balance laws from first principles. As is well-known, for stress-energy conservation, these first principles are spacetime symmetries (approximate *local* Poincaré invariance in the case of general relativity). We have not found a clear derivation from first principles for the kinematic conservation laws of elasticity in either the Newtonian or relativistic literature, and therefore give one here. We find the spacetime point of view helpful even in Newtonian physics. The following remarks do not refer to any metric on spacetime, and therefore hold identically in Newtonian physics and general relativity. (For this discussion it is also irrelevant that Newtonian spacetime has a preferred time and relativistic spacetime does not.)

The geometric meaning of the integrability conditions (11) is that the three 1-forms ${\psi^A}_a$ for $A = 1, 2, 3$ form hypersurfaces in spacetime. These surfaces can be interpreted as the world-volumes of crystal surfaces, and we shall call them crystal world surfaces. Their intersections with a time slice are the instantaneous crystal surfaces (locally, "crystal planes"). The lines formed by the intersection of a 1-world surface, a 2-surface and a 3-surface are particle world lines. The line formed by the intersection of a 1-surface, a 2-surface and a time slice is an instantaneous crystal 3-line (locally "crystal axis"), and so on.

Now the weak form of (11) keeps the crystal world surfaces continuous while allowing them to kink. By assumption, the time slices are also continuous (in fact smooth). Hence the weak form of (11) also keeps the world lines and instantaneous crystal lines continuous while allowing them to kink. This is the interpretation of the 3+1 split of the weak form of (11), as we shall now see. (It is irrelevant for this discussion that the world lines are geometrical invariants, while the instantaneous crystal lines are not.)

In the following, we consider the conservation laws (14) and (15), which together are equivalent to the pair (14) and (17) that we shall actually solve.

Consider a surface of discontinuity in space (from now on called a shock for briefness). Let n_i be a covector normal to the shock (uniquely defined up to an overall factor). Let s^i be the shock velocity vector (defined, in the absence of a metric, only up to the addition of a vector tangential to the shock), and let $s := s^i n_i$ (which inherits the arbitrary factor in n_i but not the arbitary vector in s^i) be the normal shock speed. The jump (Rankine-Hugoniot) conditions arising from (14) and (15) are then

$$\left[{\psi^A}_k \delta^k_{[i} \delta^l_{j]}\right] n_l = 0, \tag{19}$$

$$-s\left[{\psi^A}_i\right] + \left[\hat{v}^j {\psi^A}_j \delta^k_i\right] n_k = 0. \tag{20}$$

(Square brackets indicate the jump across the shock.)

We want to decompose these conditions into parts normal and parallel to the shock. Let n^i be a vector that obeys $n^i n_i = 1$. In the absence of a metric, n^i is therefore uniquely defined up to the factor in n_i, and the addition of an arbitrary vector tangent to the shock. Define the tensor

$${\|^i}_j := {\delta^i}_j - n^i n_j. \tag{21}$$

It is the projection operator into the tangent plane of the shock in the sense that

$${\|^i}_j \, n_i = 0, \quad {\|^i}_j \, n^j = 0, \quad {\|^i}_j \, {\|^j}_k = {\|^i}_k. \tag{22}$$

Split into normal and tangential components defined by $\hat{v}^n := v^i n_i$ and $\hat{v}^{\|i} := {\|^i}_j \hat{v}^j$, and similarly for other spatial tensors, the jump conditions can now be compactly written as

$$[{\psi^A}_{\|i}] = 0, \tag{23}$$

$$[{\psi^A}_n (\hat{v}^n - s)] + {\psi^A}_{\|i} [\hat{v}^{\|i}] = 0. \tag{24}$$

The first of these guarantees the continuity of crystal lines across the shock, or the absence of "surgery across the shock", as illustrated in Fig. 1. The second guarantees the continuity of particle world lines, and hence the conservation of particles, as they cross the shock. Consider the special case where $\hat{v}^{\|i}$ is continuous. Then, in the rest frame of the shock, $[{\psi^A}_n \hat{v}^n] = 0$. This is a pure "density" shock of the type familiar from fluid dynamics, and is illustrated in the left panel of Fig. 2. Conversely, consider the case where ${\psi^A}_n$ is continuous. Then, again in the rest frame of the shock,

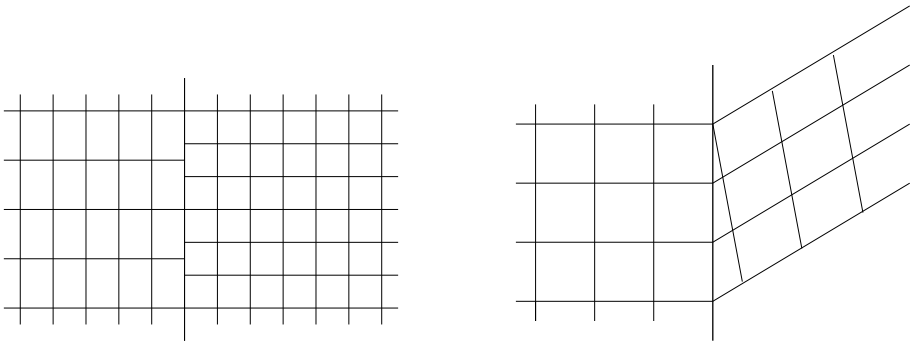

Figure 1: Discontinuities of the types illustrated here are not allowed by the jump conditions (it would require "surgery" on the material). For simplicity and without loss of generality, we choose space and matter space coordinates in this and the next figure so that the shock is along the y axis and ${\psi^A}_i = \delta^A_i$ in the left state. The type of surgery in the left panel is then forbidden by $[{\psi^Y}_y] = 0$. The type of surgery in the right panel is forbidden by $[{\psi^X}_y] = 0$.

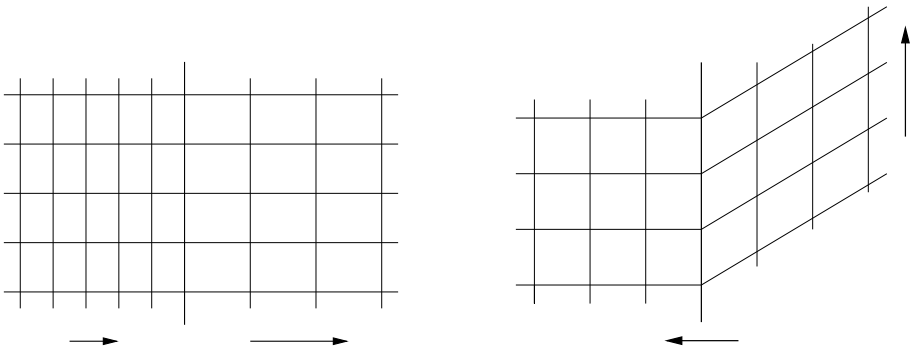

Figure 2: The left panel shows a pure density shock, with v^y continuous, shown in the rest frame of the shock. This is essentially a one-dimensional phenomenon. "Density" and velocity on the left and right (shown as arrows) are related (in these coordinates) by $[{\psi^X}_x v^x] = 0$. The right panel shows a pure travelling kink, shown in the rest frame of the left state. For simplicity, we have assumed ${\psi^X}_x = 1$ to be continuous in this example, which implies that $v^x = 0$ is continuous and the "volume density" is continous. However, the "line density" along the Y crystal axis is discontinuous. The shock speed and shear speed (shown as arrows) in these coordinates are related by $s({\psi^Y}_x)_R = (v^y)_R$.

${\psi^A}_n[\hat{v}^n] + {\psi^A}_{\|i}[\hat{v}^{\|i}] = 0$. This is a pure travelling kink, set up by a discontinuity in the tangential velocity, as illustrated in the right panel of Fig. 2.

Fluids allow for a contact discontinuity where the tangential velocity jumps. In elastic matter, this is replaced by the travelling kink. The only contact discontinuity that survives is one where the entropy jumps. This holds even in the limit where the dynamics goes to the fluid limit (the stiffness goes to zero and the stress-energy tensor becomes that of a fluid), and so the fluid limit is singular.

2.4. Matter space metric and particle number current

The minimal geometric structure on matter space is a volume form n_{ABC} whose integration over a volume in matter space gives the number of particles in that part of matter space. To model elasticity, at least a conformal metric is required in addition to define angles on matter space, which can then be compared with angles on spacetime to define deformations. But together these two structures define a full Riemannian metric k_{AB}. ("Distances" measured by this metric are in particles, not meters). Therefore we now assume that k_{AB} is defined and n_{ABC} is compatible with it. In matter coordinates ξ^A this means that

$$n_{ABC} = \sqrt{k_\xi}\, \delta_{ABC}, \tag{25}$$

where

$$k_\xi := \frac{1}{3!}\delta^{ABC}\delta^{DEF}k_{AD}\, k_{BE}\, k_{CF} \tag{26}$$

is the usual determinant. The suffix ξ is a reminder that it is not a scalar on matter space but depends on the ξ^A coordinates.

We use k_{AB} as an example to discuss tensors on matter space and their pull-back to spacetime. Matter space itself has no time, but as we are using a Eulerian framework, we effectively consider $k_{AB}(\chi^C(x^d))$ as a function on spacetime. Furthermore, we can define the pull-back of k_{AB} to a tensor k_{ab} on spacetime as

$$k_{ab} := \psi^A{}_a \psi^B{}_b k_{AB}. \tag{27}$$

From this definition alone, we see that

$$\mathcal{L}_u k_{ab} = 0, \quad u^a k_{ab} = u^b k_{ab} = 0. \tag{28}$$

Formally, tensor fields on matter space could therefore be defined as tensors on spacetime whose Lie derivative along u^a and contractions with u^a all vanish, and this is indeed the approach of [8], and partly of [9]. However, equivalently the components $k_{AB}(\chi^C(x^d))$ can be considered as scalars on spacetime that are constant along particle world lines, so that

$$u^a k_{AB,a} = 0, \tag{29}$$

or in coordinates

$$k_{AB,t} + \hat{v}^i k_{AB,i} = 0. \tag{30}$$

Numerically, we prefer to work with k_{AB}, which has fewer components and a simpler evolution equation than k_{ab}.

Following [8, 9], we consider the pull-back of n_{ABC} to a 3-form n_{abc} on spacetime

$$n_{abc} := \psi^A{}_a \psi^B{}_b \psi^C{}_c n_{ABC}. \tag{31}$$

Spacetime also has a volume form ϵ_{abcd}, compatible with a Lorentzian metric g_{ab}. In arbitrary coordinates,

$$\epsilon_{abcd} = \sqrt{g_x}\, \delta_{abcd}, \quad g_x := -\frac{1}{4!}\delta^{abcd}\delta^{efgh} g_{ae}\, g_{bf}\, g_{cg}\, g_{dh}. \tag{32}$$

(We have defined g_x as positive for ease of notation). We then define the particle number current

$$j^a := \frac{1}{3!}\epsilon^{abcd} n_{bcd}. \tag{33}$$

This is timelike, and conserved,

$$\nabla_a j^a = \epsilon^{abcd} \nabla_a n_{bcd} = 0, \tag{34}$$

where ∇_a is the covariant derivative compatible with g_{ab}. The right-hand side vanishes because $n_{[BCD,A]}$ must vanish as it is a 4-form on a 3-dimensional space. We split j^a into a matter 4-velocity and a particle density

$$j^a =: n u^a, \tag{35}$$

where u^a is normalised as

$$u^a u_a = -1 \tag{36}$$

(and hence $n = -j_a j^a$). In coordinates, using (A.2) and (A.12), $\nabla_a j^a = 0$ becomes

$$\left(\sqrt{\gamma_x} W n\right)_{,t} + \left(\sqrt{\gamma_x} W n \hat{v}^i\right)_{,i} = 0. \tag{37}$$

Conversely, we can relate the particle density and current via $n = -u_a j^a$, and substituting (A.13) into this and using (A.3), we obtain

$$n = \frac{1}{3!} W^{-1} \epsilon^{ijk} n_{ijk} = \frac{\sqrt{k_\xi}\psi_{x\xi}}{W\sqrt{\gamma_x}}. \tag{38}$$

Here n_{ijk} are the space components of the 4-dimensional 3-form n_{abc} in the adapted coordinates (t, x^i), and $\psi_{x\xi}$ is the determinant

$$\psi_{x\xi} := \frac{1}{3!} \delta^{ijk} \delta_{ABC} \psi^A{}_i \psi^B{}_j \psi^C{}_k. \tag{39}$$

We now show explicitly that $\nabla_a j^a = 0$ is a linear combination of the evolution equations (18) for $\psi^A{}_i$, that is, the kinematic evolution equations *with* the hyperbolicity fix. Contracting (18) with $F^i{}_A$, the matrix inverse of $\psi^A{}_i$, and using the matrix identity $\delta(\ln \psi_{x\xi}) = F^i{}_A \delta \psi^A{}_i$, we obtain

$$(\ln \psi_{x\xi})_{,t} + \hat{v}^i (\ln \psi_{x\xi})_{,i} + \hat{v}^i{}_{,i} = 0. \tag{40}$$

Working from the other end, we insert (38) and (9) into (35) and use (A.2) to obtain

$$j^a = \frac{\sqrt{k_\xi}\psi_{x\xi}}{\sqrt{g_x}} (1, \hat{v}^i). \tag{41}$$

Hence $\nabla_a j^a = 0$ is equivalent to

$$(\sqrt{k_\xi}\psi_{x\xi})_{,t} + (\sqrt{k_\xi}\psi_{x\xi}\hat{v}^i)_{,i} = 0. \tag{42}$$

But with the advection equation

$$(k_\xi)_{,t} + \hat{v}^i (k_\xi)_{,i} = 0, \tag{43}$$

which follows from (30), this is equivalent to (40).

3. Relativistic dynamics

3.1. Action and stress-energy tensor

We begin with the matter action

$$S := \int e(g^{ab}, \psi^A{}_a, k_{AB}, \ldots, s)\, g_x^{1/2}\, d^4x, \tag{44}$$

where the dots stand for any other tensors on matter space and s is the entropy per rest mass. In the absence of shocks, s is constant on particle world lines, and so can be considered as a scalar on matter space. We shall see later that the Lagrangian density e evaluates to the total energy density for configurations that are solutions of the Euler-Lagrange equations. Varying for now only the metric, the standard definition of the stress-energy tensor T_{ab}, namely

$$\delta S =: \frac{1}{2} \int T_{ab}\ \delta g^{ab}\ g_x^{1/2}\, d^4x, \tag{45}$$

evaluates to

$$T_{ab} = 2\frac{\partial e}{\partial g^{ab}} - e g_{ab}. \tag{46}$$

We define a projector into the tangent space normal to the 4-velocity,

$$h_{ab} := u_a u_b + g_{ab}. \tag{47}$$

(h_{ab} should not be confused with the projector γ_{ab} into the $t =$ const hypersurfaces defined in (A.7).)

We can now write

$$T_{ab} = e u_a u_b + p_{ab}, \tag{48}$$

where

$$p_{ab} := 2\frac{\partial e}{\partial g^{ab}} - e h_{ab}, \tag{49}$$

which is by definition symmetric. We shall later see that p_{ab} encodes the stresses (the isotropic pressure and the anisotropic stress).

We define the push-forward of the inverse spacetime metric to matter space,

$$g^{AB} := \psi^A{}_a \psi^B{}_b g^{ab}. \tag{50}$$

We define g_{AB} as its matrix inverse. We therefore now have two Riemannian metrics on matter space, namely g_{AB} and k_{AB}. Note that g_{AB} transforms as a tensor under coordinate changes on matter space (and as a scalar under coordinate changes on spacetime), but it explicitly depends on the deformation of the matter, and is therefore "time-dependent". By contrast k_{AB} is a genuine tensor on matter space alone. As a matter of convention and terminology, we will therefore refer to k_{AB} (only) as *the* matter space metric, but we will later implicitly move matter space indices with g_{AB} and g^{AB} *as if* it was a metric (and never implicitly with k_{AB}). Note that in this convention $k^{AB} := g^{AC} g^{BD} k_{BD}$, and that this is *not* the matrix inverse of k_{AB}. (We note in passing that the Newtonian limit $\psi^A{}_i \psi^B{}_j \gamma^{ij}$ of g^{AB}, where γ^{ij} is the metric of Newtonian space, is commonly called the Finger tensor in the Newtonian literature. The Newtonian literature implicitly assumes that k_{AB} and γ_{ij} are flat and given in Cartesian coordinates and moves indices implicitly. Moreover, some expressions can only be made sense of if $F^i{}_A$ and $\psi^A{}_i$ are also used implicitly to convert between space and matter space indices.)

As a further illustration of these conventions, the quantity

$$\psi_A{}^a := \psi^B{}_b g^{ab} g_{AB} \tag{51}$$

is the inverse of $\psi^A{}_a$ (which is not a square matrix, and so has no matrix inverse) in the sense that

$$\psi^A{}_a \psi_B{}^a = \delta^A{}_B, \tag{52}$$

$$\psi^A{}_a \psi_A{}^b = h_a{}^b. \tag{53}$$

(The first of these follows directly from the definition of g_{AB} as the matrix inverse of g^{AB}. The second can be shown by verifying that the right-hand side is normal to u^a and u_b, and obeys $h_a{}^b h_b{}^c = h_a{}^c$.)

From covariance in both spacetime and matter space, we must have

$$e(\psi^A{}_a, g^{ab}) = e(g^{AB}), \tag{54}$$

as this is the only way the spacetime indices on $\psi^A{}_a$ and g^{ab} can be contracted. (A more formal proof is given in [10].) Hence

$$\frac{\partial e}{\partial g^{ab}} = \frac{\partial e}{\partial g^{AB}} \frac{\partial g^{AB}}{\partial g^{ab}} = \frac{\partial e}{\partial g^{AB}} \psi^A{}_a \psi^B{}_b. \tag{55}$$

Hence $p_{ab} u^a = 0$, and so $u_a h_{bc} T^{ab} = 0$. This means that there is no energy flux relative to the matter. In this sense we are dealing with ideal (non-dissipative) elastic matter. p_{ab} is called the pressure tensor (for a perfect fluid, $p_{ab} = p h_{ab}$, where p is the pressure), and we now see that the Lagrangian e in the action (44) evaluates (for solutions to the Euler-Lagrange equations) to the total energy density (in the rest frame of the matter).

We next note that

$$n^2 = \frac{1}{3!} n^{abc} n_{abc} = \frac{1}{3!} g^{ad} g^{be} g^{cf} n_{abc} n_{def}. \tag{56}$$

From its relation to the matter space volume form (31), n_{abc} is independent of g^{ab} in the sense that it is constructed only from n_{ABC} and $\psi^A{}_a$. Hence, taking a derivative of (56),

$$\frac{\partial n}{\partial g^{ab}} = \frac{1}{2} n h_{ab}, \tag{57}$$

where in the partial derivative n is considered as a function of g^{ab}, $\psi^A{}_a$ and the matter tensors, as well as s. Then, defining ϵ by

$$e =: n(1 + \epsilon), \tag{58}$$

we have

$$p_{ab} = 2n \frac{\partial \epsilon}{\partial g^{ab}}, \tag{59}$$

with the same definition of the partial derivative. ([9] and [10] define $e = n\epsilon$. Here we take the rest mass out of the energy density to agree with the usual definition of ϵ in relativistic hydrodynamics as the *internal* energy per rest mass.) Similarly to (55), we can write (59) as

$$p_{ab} = n \tau_{AB} \psi^A{}_a \psi^B{}_b, \tag{60}$$

where we have defined

$$\tau_{AB} := 2 \frac{\partial \epsilon}{\partial g^{AB}}. \tag{61}$$

(The Newtonian limit of τ_{AB} is commonly called the second Piaola-Kirchhoff tensor in the Newtonian literature, modulo the implicit assumptions mentioned above.)

3.2. Isotropic matter

We now specialise to the case that the specific internal energy ϵ depends on g^{ab}, ${\psi^A}_a$, s and a single matter tensor, the metric k_{AB}. (Modelling matter with an anisotropic crystal structure would require e to depend on additional tensor fields on matter space, such as a preferred frame.) e and hence ϵ should transform as a scalar both on spacetime and on matter space. We therefore need to find all double scalars that can be made from g^{AB} and k_{AB}.

From (50), we see that g^{AB} transforms as a (2,0)-tensor on matter space and as a scalar on spacetime. With this in mind we define

$$ {k^A}_B := g^{AC}k_{BC} = g^{ac}{\psi^A}_a{\psi^C}_c k_{BC}. \tag{62} $$

This transforms as a scalar on spacetime and as a $(1,1)$ tensor on matter space. Hence its eigenvalues transform as scalars on matter space. They are the required double scalars. (We note that [9] work with the (1,1)-tensor on spacetime ${k^a}_b = g^{ac}{\psi^B}_b{\psi^C}_c k_{BC}$ instead. This has the same eigenvalues as ${k^A}_B$ in addition to one zero eigenvalue.)

We split the matrix ${k^A}_B$ into its determinant k and a unit determinant matrix ${\eta^A}_B$,

$$ {\eta^A}_B := k^{-1/3}{k^A}_B, \tag{63} $$

and note that the determinant is related to the particle density by

$$ \begin{aligned} k &:= \frac{1}{3!}\delta_{ABC}\delta^{DEF}{k^A}_D\,{k^B}_E\,{k^C}_F \\ &= \delta^D_{[A}\delta^E_B\delta^F_{C]}{k^A}_D\,{k^B}_E\,{k^C}_F \\ &= g^{[A|D}k_{AD}\;g^{|B|E}k_{BE}\;g^{|C]F}k_{CF} \\ &= \frac{1}{3!}g^{AD}g^{BE}g^{CF}n_{ABC}n_{DEF} \\ &= n^2, \end{aligned} \tag{64} $$

where the first equality is the usual definition of the determinant of a matrix, the second reminds us that for a (1,1)-tensor this is actually a scalar, the third is the definition of ${k^A}_B$, the fourth follows from the fact that n_{ABC} is the volume form of k_{AB}, and the last one is (56) pushed forward to matter space.

We can now consider the specific internal energy ϵ as a function of n, ${\eta^A}_B$ and s. In fact, it can depend on ${\eta^A}_B$ only through its scalar invariants, of which there are precisely two independent ones. Hence

$$ \epsilon({k^A}_B, s) = \epsilon(k, {\eta^A}_B, s) = \epsilon(n, I^1, I^2, s), \tag{65} $$

where $n = k^{1/2}$ as just shown and we have defined

$$ I^1 := {\eta^A}_A = k^{-1/3}g^{AB}k_{AB}, \tag{66} $$

$$ I^2 := {\eta^A}_B{\eta^B}_A = k^{-2/3}g^{AB}g^{CD}k_{AC}k_{BD}. \tag{67} $$

(See Appendix H for a definition of other choices of shear invariants.) With g_{AB} defined as the matrix inverse of g^{AB} we have

$$ \frac{\partial k}{\partial g^{AB}} = k\,g_{AB}, \tag{68} $$

and hence

$$ \frac{\partial n}{\partial g^{AB}} = \frac{1}{2}n\,g_{AB}. \tag{69} $$

We find

$$\tau_{AB} = \frac{p}{n} g_{AB} + 2(f_1 \pi^1_{AB} + f_2 \pi^2_{AB}), \tag{70}$$

where

$$p \quad := n^2 \frac{\partial \epsilon}{\partial n}, \tag{71}$$

$$f_{1,2} := \frac{\partial \epsilon}{\partial I^{1,2}}, \tag{72}$$

$$\pi^1_{AB} := \frac{\partial I^1}{\partial g^{AB}} = \eta_{AB} - \frac{1}{3} g_{AB} I^1, \tag{73}$$

$$\pi^2_{AB} := \frac{\partial I^2}{\partial g^{AB}} = 2(\eta_{AC} \eta^C{}_B - \frac{1}{3} g_{AB} I^2). \tag{74}$$

Substituting (70) into (60), we see that

$$p_{ab} = p h_{ab} + \pi_{ab}, \tag{75}$$

with the first term the stress tensor of a perfect fluid and the second term representing the anisotropic stress,

$$\pi_{ab} = \psi^A{}_a \psi^B{}_b \pi_{AB}, \tag{76}$$

where

$$\pi_{AB} := 2n(f_1 \pi^1_{AB} + f_2 \pi^2_{AB}). \tag{77}$$

Hence π_{ab} is a tracefree spatial tensor in the sense that

$$\pi_{ab} u^a = 0, \qquad h^{ab} \pi_{ab} = 0. \tag{78}$$

Moreover, π_{ab} vanishes if ϵ depends only on n and s, which is the fluid limit.

We also note that with the temperature defined by

$$T := \frac{\partial \epsilon}{\partial s}, \tag{79}$$

the first law of thermodynamics on a per particle basis can be written as

$$d\epsilon = T\, ds - p\, d\left(\frac{1}{n}\right) + f_1\, dI^1 + f_2\, dI^2, \tag{80}$$

so $f_{1,2}$ are the "generalised forces" in the thermodynamical sense associated with the intensive thermodynamics variables $I^{1,2}$.

3.3. The unsheared state

Elastic matter at a given density n has an *unsheared* state that minimises ϵ at fixed n, but one cannot assume that there exists a *relaxed* state that minimises ϵ absolutely, including under variation of n. This is because at sufficiently low pressure, and hence n, the matter may be in a fluid rather than solid state [9].

It is intuitively clear that the unsheared state corresponds to $\eta^A{}_B = \delta^A{}_B$. In fact, we see from (73,74) that π_{ab} vanishes for all values of $\psi^A{}_a$ if and only if $\eta^A{}_B = \delta^A{}_B$. This means that η_{AB} is the matrix inverse of g^{AB}, or

$$\eta_{AB} = g_{AB}. \tag{81}$$

Hence

$$k_{AB} = n^{2/3}\, g_{AB} \tag{82}$$

in the unsheared state. It is natural to assume that matter freezes in the unsheared state. Hence we set k_{AB} to (82) at the moment of freezing, and advect it via (30) afterwards. Note that the pull-back of g_{AB} to spacetime is h_{ab}, which even in special relativity is not flat, so in general k_{AB} will not be flat, except in the Newtonian limit where $h_{ab} = \gamma_{ab}$ is flat and even then only if n takes a constant value at freezing.

4. Hyperbolicity

4.1. Overview

For smooth solutions, it is natural to consider the relativistic elasticity equations as a system of second-order PDEs in the variables $\chi^A(x^a)$. In order to show existence and uniqueness of solutions, Beig and Schmidt [10] have introduced an explicit reduction to first order of these equations, and have shown that the reduction is a first-order symmetric hyperbolic system, at least in the unsheared state.

The reduction of any second-order system to first-order hyperbolic form is complicated by the fact that the reduction creates definition constraints on the auxiliary variables (here, $\psi^A{}_{[i,j]} = 0$), which can be added to the evolution equations to change their principal part and hence their hyperbolicity properties. (We note in this context that in [20] a *definition* of symmetric hyperbolicity for a second-order system has been given as the existence of a symmetric hyperbolic reduction to first, together with a *necessary and sufficient criterion* for this reduction to exist, which is purely algebraic in terms of the principal symbol of the second-order system. Hence if well-posedness of the second-order system is the only concern, constructing an explicit first-order reduction is unnecessary.)

We have a different reason for constructing an explicit first-order reduction: we want to construct a numerical scheme that can accurately reproduce weak solutions of the relativistic elasticity equations. As for weak solutions of fluid mechanics, the standard way of doing this is to construct HRSC numerical schemes for the equations in an appropriate first-order balance law form.

In this section we will show that the kinematic evolution equations (17), together with dynamical evolution equations of the form $\nabla_b T^{ab} =$ (constraints), form a symmetric hyperbolic system of evolution equations for $\psi^A{}_a$, or equivalently $\psi^A{}_i$ and $\hat{v}^i$, if the constraints (12) are obeyed or not. We also show that (17), together with just $\nabla_b T^{ab} = 0$, as used in the Newtonian formalisms [12, 13, 14, 21], is strongly hyperbolic but not symmetric hyperbolic.

For completeness, relevant standard definitions of hyperbolicity are summarised in Appendix B.

4.2. The second-order system

Roughly speaking, the first-order equations for $\psi^A{}_a$ must be the second-order equations for χ^A, replacing $\chi^A{}_{,ab}$ by $\psi^A{}_{a,b}$ and adding multiples of the constraint $\psi^A{}_{[a,b]}$ to the right-hand sides. We therefore derive the second-order equations first, following [10]. In particular, this will allow us to establish the standard connection between the matter evolution equations and stress-energy conservation.

Hence, in this subsection we consider g^{ab} and χ^A as the independent variables. We consider $\psi^A{}_a = \chi^A{}_{,a}$ as a derived object, and we consider k_{AB}, any other matter

space tensors, and s, as fixed tensor fields on matter space that are not varied in the following. The action is

$$S := \int e(g^{ab}, \chi^A, \chi^A{}_{,a}, k_{AB}, \ldots, s)\, \sqrt{g_x}\, d^4x. \tag{83}$$

After integration by parts, and neglecting the boundary terms, its variation is

$$\delta S = \int \left(\frac{1}{2} T_{ab}\ \delta g^{ab} + \mathcal{E}_A\ \delta \chi^A \right) \sqrt{g_x}\, d^4x, \tag{84}$$

where the stress-energy tensor is given as before by (46), and the Euler-Lagrange equations are

$$\mathcal{E}_A := \frac{\partial e}{\partial \chi_A} - \frac{1}{\sqrt{g_x}} \left(\sqrt{g_x} \frac{\partial e}{\partial (\chi^A{}_{,a})} \right)_{,a}. \tag{85}$$

Note that these are second-order differential equations for χ^A.

Variations generated by an infinitesimal change of coordinates $x^a \to x^a + \zeta^a$ on the spacetime take the form

$$\delta \chi^A = \mathcal{L}_\zeta \chi^A = \zeta^c \psi^A{}_c, \tag{86}$$

$$\delta g^{ab} = \mathcal{L}_\zeta g^{ab} = 2\nabla^{(a} \zeta^{b)}. \tag{87}$$

The action must be invariant under such changes, and hence after another integration by parts

$$\nabla^b T_{ab} = \psi^A{}_a \mathcal{E}_A. \tag{88}$$

Hence stress-energy conservation holds if and only if the elastic matter field equations hold. In one direction, this is not immediately obvious as $\mathcal{E}_A = 0$ has only three independent components, while $\nabla^b T_{ab} = 0$ has four. However, $u^a \nabla^b T_{ab} = 0$ is equivalent to

$$n \left(\dot{\epsilon} - \frac{p}{n^2} \dot{n} \right) + \pi^{ab} \nabla_a u_b = 0, \tag{89}$$

where a dot denotes $u^a \nabla_a$. But this is just the first law (80), evaluated along a particle worldline, for smooth solutions, so that $\dot{s} = 0$. Hence it is an identity if the stress-energy tensor is thermodynamically consistent with the equation of state.

The matter equations in their second-order form can be written as

$$\mathcal{E}_A = M^{ab}{}_{AB} \chi^B{}_{,ba} - G_A = 0 \tag{90}$$

where

$$M^{ab}{}_{AB} := \frac{\partial^2 e}{\partial \psi^A{}_a \partial \psi^B{}_b} \tag{91}$$

are the coefficients of the principal part and G_A comprises all lower-order terms. From its definition,

$$M^{ab}{}_{AB} = M^{ba}{}_{BA}. \tag{92}$$

We shall see that $M^{ab}{}_{AB}$ as defined by (91) is not symmetric in ab alone, even though $M^{[ab]}{}_{AB}$ does not contribute to (90). We note in passing that the second-order system with principal part $M^{ab}{}_{AB}$ is "regular hyperbolic" in the sense of [29].

4.3. The principal symbol

We shall write the principal symbol more explicitly in terms of the shear and the equation of state. From (54),

$$M^{ab}{}_{AB} = 4\frac{\partial^2 e}{\partial g^{AC}\partial g^{BD}}\psi^{Ca}\psi^{Db} + 2\frac{\partial e}{\partial g^{AB}}g^{ab}, \tag{93}$$

where we have defined

$$\psi^{Aa} := \psi^{A}{}_{b}g^{ab}. \tag{94}$$

With

$$g^{ab} = -u^a u^b + \psi^{Aa}\psi^{Bb}g_{AB}, \tag{95}$$

this can be split into parts parallel and normal to the 4-velocity as

$$M^{ab}{}_{AB} = -\mu_{AB}u^a u^b + U_{ACBD}\psi^{Ca}\psi^{Db}, \tag{96}$$

where

$$\mu_{AB} := 2\frac{\partial e}{\partial g^{AB}}, \tag{97}$$

$$U_{ACBD} := 4\frac{\partial^2 e}{\partial g^{AC}\partial g^{BD}} + 2\frac{\partial e}{\partial g^{AB}}g_{CD}. \tag{98}$$

Note that there are no cross terms, that is $u_a h_{bc}M^{ab}{}_{AB} = 0$.

We now evaluate the symbols μ_{AB} and U_{ACBD} further. With (58), using (69), we can rewrite

$$\mu_{AB} = n\tau_{AB} + eg_{AB}, \tag{99}$$

$$U_{ACBD} = n\big(g_{AC}\tau_{BD} + g_{BD}\tau_{AC} + \tau_{AB}g_{CD} + \tau_{ACBD}\big) + 2eg_{A[C}g_{D]B}, \tag{100}$$

where τ_{AB} was defined above in (61), and analogously we have defined

$$\tau_{ABCD} := 4\frac{\partial^2 \epsilon}{\partial g^{AB}\partial g^{CD}}. \tag{101}$$

Using the chain rule, we now express τ_{AB} and τ_{ABCD} as a sum of terms, each of which is a product of a matter scalar (such as e, p, c_s^2 etc.) and a tensor that depends only on the deformation. We can rewrite the expression (70) for τ_{AB} more compactly as

$$\tau_{AB} = \frac{p}{n}g_{AB} + 2f_\alpha \pi^\alpha_{AB}, \tag{102}$$

where $\alpha = 1, 2$ labels the shear invariants, and we use a summation convention over α. With the same notation, we can write

$$\begin{aligned}\tau_{ABCD} = &-2\frac{p}{n}g_{A(C}g_{D)B} + \left(c_s^2 - \frac{p}{n}\right)g_{AB}g_{CD} \\ &+ 2n\left(g_{AB}f_{n\alpha}\pi^\alpha_{CD} + g_{CD}f_{n\alpha}\pi^\alpha_{AB}\right) \\ &+ 4f_{\alpha\beta}\pi^\alpha_{AB}\pi^\beta_{CD} + 4f_\alpha \pi^\alpha_{ABCD},\end{aligned} \tag{103}$$

where

$$c_s^2 := \frac{\partial p}{\partial n}, \qquad f_{n\alpha} := \frac{\partial^2 \epsilon}{\partial n \partial I^\alpha}, \qquad f_{\alpha\beta} := \frac{\partial^2 \epsilon}{\partial I^\alpha \partial I^\beta}, \tag{104}$$

and

$$\begin{aligned}\pi^1_{ABCD} &:= \frac{\partial^2 I^1}{\partial g^{AB}\partial g^{CD}}\\ &= \left(\frac{1}{3}g_{A(C}g_{D)B}+\frac{1}{9}g_{AB}g_{CD}\right)I^1\\ &\quad -\frac{1}{3}(\eta_{AB}g_{CD}+\eta_{CD}g_{AB}),\end{aligned} \tag{105}$$

$$\begin{aligned}\pi^2_{ABCD} &:= \frac{\partial^2 I^2}{\partial g^{AB}\partial g^{CD}}\\ &= \left(\frac{2}{3}g_{A(C}g_{D)B}+\frac{4}{9}g_{AB}g_{CD}\right)I^2\\ &\quad -\frac{4}{3}(\eta_{AE}\eta^E{}_Bg_{CD}+\eta_{CE}\eta^E{}_Dg_{AB})\\ &\quad +2\eta_{A(C}\eta_{D)B}.\end{aligned} \tag{106}$$

4.4. The unsheared state

The principal symbol simplifies considerably in the unsheared state, denoted by a circle, where

$$\mathring{I}^\alpha = 3, \tag{107}$$

$$\mathring{\pi}^\alpha_{AB} = 0, \tag{108}$$

$$\mathring{\pi}^1_{ABCD} = g_{A(C}g_{D)B}-\frac{1}{3}g_{AB}g_{CD}, \tag{109}$$

$$\mathring{\pi}^2_{ABCD} = 4\pi^1_{ABCD}, \tag{110}$$

and therefore

$$n\mathring{\tau}_{AB} = pg_{AB}, \tag{111}$$

$$n\mathring{\tau}_{ABCD} = 2r\,g_{A(C}g_{D)B}+q\,g_{AB}g_{CD}, \tag{112}$$

where

$$r := -p+2n(f_1+4f_2), \tag{113}$$

$$q := nc_s^2-p-\frac{4}{3}n(f_1+4f_2). \tag{114}$$

Note that in the unsheared state only the combination f_1+4f_2 appears.

We finally obtain

$$\mathring{\mu}_{AB} = (p+e)g_{AB}, \tag{115}$$

$$\begin{aligned}\mathring{U}_{ACBD} &= (2p+q+e)g_{AC}g_{BD}+(p+r)g_{AB}g_{CD}\\ &\quad +(r-e)g_{AD}g_{BC}.\end{aligned} \tag{116}$$

(This reduces to Eq. (4.16) of [10] in the special case $p=\epsilon=0$.)

4.5. First-order systems

Any first-order reduction of the second-order system must have the form

$$\bar{\mathcal{E}}_A := \bar{M}^{ab}{}_{AB}\psi^B{}_{b,a}-G_A = 0 \tag{117}$$

with

$$\bar{M}^{ab}{}_{AB} := M^{ab}{}_{AB} + D^{ab}{}_{AB}, \tag{118}$$

where

$$D^{ab}{}_{AB} = D^{[ab]}{}_{AB} \tag{119}$$

governs constraint addition. Note that as a matter of convention, $M^{ab}{}_{AB}$ is the tensor defined by (91) (with a specific, as it happens nonzero, antisymmetric in ab part), whereas $\bar{M}^{ab}{}_{AB}$ denotes a tensor with the same symmetric in ab part but a different, yet unspecified antisymmetric in ab part.

In particular, $\nabla_b T^{ab} = 0$ should give us the dynamical part of the equations, but as we shall see, in order to achieve symmetric hyperbolicity of the entire system, we will have to add constraints to these equations. It turns out that adding constraints only to the "spatial" part of $M^{ab}{}_{AB}$ is sufficient. Hence, we consider the evolution equations

$$\bar{E}^a := \nabla_b T^{ab} + \bar{\Lambda}_{ACBD}\psi^{Aa}\psi^{Cc}\psi^{Db}\psi^{B}{}_{[b,c]} = 0, \tag{120}$$

where

$$\bar{\Lambda}_{ACBD} = -\bar{\Lambda}_{ADBC} \tag{121}$$

parameterises a family of constraint additions. To write $\nabla_b T^{ab}$ in terms of $\psi^A{}_a$, we start from

$$T^{ab} = 2\frac{\partial e}{\partial g^{AB}}\psi^{Aa}\psi^{Bb} - e g^{ab}. \tag{122}$$

Keeping only the principal part in the matter variables, that is terms of the form $\psi^B{}_{b,c}$, we find after some calculation that

$$\nabla_b T^{ab} = \left(\psi^{Aa} M^{cb}{}_{AB} - 4\frac{\partial e}{\partial g^{AB}}\psi^{A[b}g^{c]a}\right)\psi^B{}_{b,c} + \text{l.o.} \tag{123}$$

Substituting (95) into (123), we find that

$$\bar{E}^a = \left(\psi^{Aa}\bar{M}^{cb}{}_{AB} + 2u^a\mu_{AB}\psi^{A[b}u^{c]}\right)\psi^B{}_{b,c} + \text{l.o.}, \tag{124}$$

where

$$\bar{M}^{ab}{}_{AB} := M^{ab}{}_{AB} + (\bar{\Lambda}_{ACDB} - 2g_{A[C}\mu_{D]B})\psi^{Ca}\psi^{Db}. \tag{125}$$

The modification of $M^{ab}{}_{AB}$ can be pushed forward to a modification of U_{ACBD}, namely

$$\bar{U}_{ACBD} := U_{ACBD} + \bar{\Lambda}_{ACDB} - 2g_{A[C}\mu_{D]B} \tag{126}$$

Splitting $\bar{E}^a$ into its parts parallel and normal to the 4-velocity, we have

$$u_a\bar{E}^a = -2\mu_{AB}\psi^{Ab}u^c\psi^B{}_{[b,c]}, \tag{127}$$

$$\psi^A{}_a\bar{E}^a = \bar{M}^{cb}{}_{AB}\psi^B{}_{b,c} - G^A. \tag{128}$$

But if μ_{AB} is invertible, $u_a\bar{E}^a = 0$ is equivalent to the kinematic evolution equations *with* hyperbolicity fix (17).

4.6. Symmetric hyperbolicity

The definition of symmetric hyperbolicity for a general system of first-order evolution equations is reviewed in Appendix B. Roughly speaking, the principal symbol must be symmetric, and its time component must be positive definite. We begin with the first condition.

Symmetry The principal symbol of neither (117) nor of (124) has the correct index structure $P_{\alpha\beta}{}^{c}$ in the composite index defined by $w^{\alpha} := \psi^{A}{}_{a}$. We follow the approach of Beig and Schmidt [10]. Define

$$W^{ab}{}_{AB}{}^{c} := u^{a}\bar{M}^{cb}{}_{AB} - 2u^{[c}\bar{M}^{b]a}{}_{BA} \tag{129}$$

and consider the system of first-order equations

$$\mathcal{E}^{a}{}_{A} := W^{ab}{}_{AB}{}^{c}\psi^{B}{}_{b,c} - G_{A}u^{a} = 0, \tag{130}$$

$$\mathcal{A}_{A} := -u^{c}g_{AB}\chi^{B}{}_{,c} = 0, \tag{131}$$

where χ^{A} and $\psi^{A}{}_{a}$ are now considered as independent variables, and u^{A} is defined by the $\psi^{A}{}_{a}$ through (31,33,35). It is clear that each solution χ^{A} of the second-order system generates a solution $\psi^{A}{}_{a} = \chi^{A}{}_{,a}$ of this first-order system. Beig and Schmidt [10] prove the converse, that a solution $\psi^{A}{}_{i}$ of the first-order system obeying $\psi^{A}{}_{[i,j]} = 0$ gives rise to a second-order solution χ^{A}. (The general approach of defining $W^{ab}{}_{AB}{}^{c}$ from $\bar{M}^{cb}{}_{AB}$ should work for any field theory that has preferred world lines (with 4-velocity u^{a} and labelled by coordinates ξ^{A}), in other words, a theory of particles.)

The principal symbol of this system has now the correct index structure. It is easy to see that it is symmetric, in the sense that

$$W^{ab}{}_{AB}{}^{c} = W^{ba}{}_{BA}{}^{c}, \qquad -u^{c}g_{AB} = -u^{c}g_{BA}, \tag{132}$$

if and only if $\bar{M}^{ab}{}_{AB}$ has the symmetry (92). To achieve this, we set

$$\bar{\Lambda}_{ACBD} = \Lambda_{ADBC} + 2g_{A[C}\mu_{D]B}, \tag{133}$$

where Λ_{ADBC} has the symmetries

$$\Lambda_{ACBD} = \Lambda_{BDAC} = -\Lambda_{ADBC}, \tag{134}$$

and will be determined when we consider positivity of the principal symbol below.

We now verify that the system (130,131) is equivalent to our evolution equations. From (96) and (125), we find

$$u_{a}\bar{M}^{ab}{}_{AB} = u^{b}\mu_{AB} \tag{135}$$

and hence

$$u_{a}W^{ab}{}_{AB}{}^{c} = -\bar{M}^{cb}{}_{AB}, \tag{136}$$

$$\psi_{Ca}W^{ab}{}_{AB}{}^{c} = -2\psi^{D[b}u^{c]}U_{ACBD}. \tag{137}$$

If U_{ACBD} is invertible as a matrix with composite indices AC and BD, we finally have the decomposition

$$u_{a}\mathcal{E}^{a}{}_{A} = 0 \quad \Leftrightarrow \quad \bar{M}^{cb}{}_{AB}\psi^{B}{}_{b,c} = G_{A}, \tag{138}$$

$$\psi^{E}{}_{a}\mathcal{E}^{a}{}_{A} = 0 \quad \Leftrightarrow \quad u^{b}\psi^{A}{}_{[a,b]} = 0, \tag{139}$$

$$\mathcal{A}_{A} = 0 \quad \Leftrightarrow \quad u^{a}\chi^{C}{}_{,a} = 0, \tag{140}$$

We see that (138) and (139) are the same as (127), (128) in our formalism. Finally, (140) is equivalent to (29) (plus similar equations for any other matter tensors), as

$$u^{a}k_{AB,a} = k_{AB,C}\,u^{a}\chi^{C}{}_{,a} \tag{141}$$

by the chain rule.

Positive definiteness The second condition for symmetric hyperbolicity is the existence of a timelike covector t_a, called a subcharacteristic vector, which makes the quadratic form (energy norm)

$$E := t_c \left(W^{ab}{}_{AB}{}^{c} m^A{}_a m^B{}_b - u^c g_{AB} l^A l^B \right) \tag{142}$$

positive definite. (The formal arguments $m^A{}_a$ and l^A of this quadratic form are in the tangent bundle of the phase space, and can be thought of as perturbations of $\psi^A{}_a$ and χ^A about a background solution.) Decomposing $m^A{}_a$ uniquely as

$$m^A{}_a =: \alpha^A u_a + \alpha^{AC} \psi_{Ca}, \tag{143}$$

and choosing $t_a = u_a$, we have

$$E = \mu_{AB} \alpha^A \alpha^B + \bar{U}_{ACBD} \alpha^{AC} \alpha^{BD} + g_{AB} l^A l^B. \tag{144}$$

Hence u_a is a subcharacteristic vector if μ_{AB} and U_{ACBD} are positive definite. (Note that then they are also invertible, as we assumed earlier.) From (115), μ_{AB} is positive definite in the unsheared state if $p + e > 0$.

It remains to look at the positive definiteness of $\bar{U}_{ACBD}$. We choose

$$\Lambda_{ACBD} = 2(d - e - p) g_{A[C} g_{D]B}, \tag{145}$$

or equivalently

$$\bar{\Lambda}_{ACBD} = 4n f_\alpha g_{A[C} \pi^\alpha_{D]B} + 2d g_{A[C} g_{D]B} \tag{146}$$

for the total constraint addition, where d is a parameter to be determined now. For simplicity, we look again at the unstrained case. Uniquely decomposing α^{AB} as

$$\alpha^{AB} = \omega^{AB} + \kappa^{AB} + \frac{\kappa}{3} g^{AB}, \tag{147}$$

where the first term is antisymmetric and the second symmetric and tracefree, we find

$$\begin{aligned} \mathring{\bar{U}}_{ACBD} \alpha^{AC} \alpha^{BD} = & \left(n c_s^2 + \frac{2d}{3} \right) \kappa^2 + d\, \omega^{AB} \omega_{AB} \\ & + \left[4n(f_1 + 4f_s) - d \right] \kappa^{AB} \kappa_{AB}. \end{aligned} \tag{148}$$

We now see that this quadratic form is positive definite, and hence our evolution equations are symmetric hyperbolic, for $0 < d < 4n(f_1 + 4f_2)$ (assuming that $c_s^2 \geq 0$). Hence, adding some constraints to $\nabla_b T^{ab} = 0$ is necessary for symmetric hyperbolicity, for example choosing for d its mid-range value $d = 2n(f_1 + 4f_2)$.

Tracing all the definitions back, we can write this particular constraint addition as

$$\bar{E}^a = \nabla_b T^{ab} + h^{ac} \psi^{Db} \left[2n f_\alpha \pi^\alpha_{DB} + 4n(f_1 + 4f_2) g_{DB} \right] \psi^B_{[b,c]}. \tag{149}$$

Looking back, the first term in the square brackets makes the principal part of the second-order system symmetric, and the second makes it positive definite.

4.7. Characteristics of the first-order system

As reviewed in Appendix B, k_a is a characteristic covector of the first-order equations with characteristic variable $w^\beta = m^B{}_b$ if

$$W^{ab}{}_{AB}{}^c m^B{}_b k_c = 0. \tag{150}$$

Once again we decompose $m^B{}_b$ in the form (143). Fixing an irrelevant overall factor, we parameterise the wave number k_a as

$$k_a = \lambda u_a - e_a, \tag{151}$$

where $e_a = \psi^A{}_a e_A$ is a unit covector on spacetime normal to u^a and e_A the corresponding unit (with respect to g^{AB}) covector on matterspace. As reviewed in Appendix B, λ is then the physical velocity of the mode relative to the matter. Using the decomposition (136,137), (150) is equivalent to the pair

$$\bar{U}_{ACBD}\left(\alpha^B e^D + \lambda \alpha^{BD}\right) = 0, \tag{152}$$

$$\lambda \mu_{AB}\alpha^B + \bar{U}_{ACBD} e^C \alpha^{BD} = 0. \tag{153}$$

Moreover, symmetric hyperbolicity implies that $\bar{U}_{ACBD}$ is invertible and so (152) is equivalent to

$$\alpha^B e^D + \lambda \alpha^{BD} = 0. \tag{154}$$

Eq. (154) has two classes of solutions. One class obeys

$$\lambda = 0, \quad \alpha^B = 0, \tag{155}$$

with α^{BD} restricted by (153) to obey

$$\bar{U}_{ACBD} e^C \alpha^{BD} = 0. \tag{156}$$

These modes travel at zero speed relative to the matter. As (156) represents 3 equations for 9 components of α^{BD}, there are 6 such modes. They can be parameterised explicitly as

$$\alpha^{BD} = (\bar{U}^{-1})^{ACBD} v_A w_C, \quad w_C e^C = 0. \tag{157}$$

The other class obeys

$$\lambda \neq 0, \quad \alpha^{BD} = -\lambda^{-1}\alpha^B e^D, \tag{158}$$

or equivalently

$$m^B{}_b = \lambda^{-1}\alpha^B k_b. \tag{159}$$

Hence $m^B{}_b$ is the gradient of a plane wave with amplitude $\lambda^{-1}\alpha^B$ and wave vector k_b, and so is a possible perturbation of $\psi^B{}_{,b}$. Hence these modes are physical, obeying the constraints. Furthermore, all physical modes are of this form, which indicates that the modes in the class (155) are all unphysical. Substituting (159) into (153), we find

$$(-\lambda^2 \mu_{AB} + \bar{U}_{ACBD} e^C e^D)\alpha^B = 0, \tag{160}$$

or equivalently

$$(-\lambda^2 \mu_{AB} + U_{ACBD} e^C e^D)\alpha^B = 0 \tag{161}$$

(constraint addition drops out). This can be written as

$$\Delta_{AB}\alpha^B = 0, \qquad \Delta_{AB} := M^{ab}{}_{AB} k_a k_b. \tag{162}$$

But, as reviewed in Appendix B, this is precisely the condition for k_a to be a characteristic covector of the second-order system with characteristic variable α^A. Hence the physical modes of the first-order system correspond one-to-one to the modes of the second-order system. There are 6 of these, forming 3 pairs with speeds $\pm\lambda$ relative to the matter.

4.8. Characteristics of the second-order system

We now look at the solutions of (162) in more detail. The general expression for Δ_{AB} is quite long, and so we begin our analysis with the unsheared state. We find

$$\mathring{\Delta}_{AB} = (-A\lambda^2 + B)g_{AB} + Ce_Ae_B, \tag{163}$$

where

$$A = e + p, \quad B = p + r, \quad C = 2p + r + q. \tag{164}$$

We can now read off the characteristic covectors and characteristic variables by inspection. Transversal waves have eigenvectors obeying $\alpha^B e_B = 0$ (and so have two polarisations travelling with the same velocity), and $\Delta_{AB}\alpha^B = 0$ then gives

$$\lambda^2 = \frac{B}{A} = \frac{2f_1 + 8f_2}{1 + \epsilon + \frac{p}{n}} =: \lambda_T^2. \tag{165}$$

Longitudinal waves have eigenvectors $\alpha^B \propto e^B$ and $\Delta_{AB}\alpha^B = 0$ gives

$$\lambda^2 = \frac{B + C}{A} = \frac{c_s^2}{1 + \epsilon + \frac{p}{n}} + \frac{4}{3}\lambda_T^2 =: \lambda_L^2. \tag{166}$$

Taking the Newtonian limit of these characteristic speeds, we can identify the shear modulus μ and the bulk modulus K as

$$\mu = n(2f_1 + 8f_2), \tag{167}$$

$$K = nc_s^2. \tag{168}$$

(These expressions hold in units where the speed of light c is one, and where n is the rest mass density, rather than the particle number density. Otherwise they have to be multiplied by c^2 and the particle mass.)

In the general, sheared, case the matter space tensor Δ_{AB} is constructed from g_{AB}, g^{AB}, $\eta_A{}^B$ and e_A. It would therefore be natural to decompose e_A (and α^B) into eigenvectors of $\eta_A{}^B$, which are automatically also eigenvectors of $g_A{}^B = \delta_A{}^B$. This can be done trivially by assuming that the index A labels that basis, so that $\eta_A{}^B$ is diagonal. The result is of the form $\Delta(\lambda) = \lambda^2\Delta_2 + \Delta_0$ (omitting the indices on Δ_{AB}). We have solved the resulting cubic equation for λ^2 by computer algebra but the result is too complicated to be illuminating.

Furthermore, for numerical purposes we are interested in the *coordinate* speeds $\lambda = dx^i/dt$ in the x^i, $i = 1, 2, 3$ direction of some Eulerian coordinate system, that is, in characteristic covectors of the form

$$k_a = \lambda(dt)_a - (dx^i)_a. \tag{169}$$

This gives a characteristic equation of the form

$$\Delta\alpha = (\lambda^2\Delta_2 + \lambda\Delta_1 + \Delta_0)\alpha = 0. \tag{170}$$

The resulting λ are not related to the characteristic speeds relative to the matter 4-velocity in a simple way, because of the appearance of the Lorentz factor W in the relativistic velocity addition. To solve (170) numerically, we use a standard linear algebra package to find the right eigenvectors $(\lambda\alpha, \alpha)^T$ and eigenvalues λ of the matrix

$$\begin{pmatrix} -(\Delta_2)^{-1}\Delta_1 & -(\Delta_2)^{-1}\Delta_1 \\ I & 0 \end{pmatrix}. \tag{171}$$

4.9. Strong hyperbolicity

In the Newtonian literature, the evolution equations for $\psi^A{}_i$ are taken to be (17) (with constraint addition), but no constraints are added to $\nabla_b T^{ab} = 0$. Our results above show that the first-order system is then definitely not symmetric hyperbolic, as the term $\bar{U}_{ACBD}$ in the principal symbol is then not positive definite even in the unsheared state, and is not symmetric in general (although it is symmetric in the unsheared state). However, the first-order system is still strongly hyperbolic if it admits a complete set of characteristic variables. We have just done the calculation in Sec. 4.7, and need to see only what changes if we cannot assume that $\bar{U}_{ACBD}$ is symmetric and positive definite.

(152) is no longer equivalent to (154) because $\bar{U}_{ACBD}$ may not have an inverse, but solutions of (154) are solutions of (152). Furthermore, (156) only admits a larger solution space if $\bar{U}_{ACBD}$ does not have maximal rank, so it will still have 6 solutions, even if they can no longer be explicitly parameterised by (157). Hence the 6 unphysical modes still exist. The 3 physical modes are completely unaffected by constraint addition (as one would expect) because we solve (161) to find them.

Hence we have proved that the first-order system consisting of (17) and $\nabla_a T^{ab} = 0$ is strongly hyperbolic (but not symmetric hyperbolic) as long as the second-order system is strongly hyperbolic.

5. Stress-energy conservation in 3+1 form

5.1. Conservation laws

The energy and momentum conservation laws in general relativity are the spacelike and timelike components of stress-energy conservation

$$\nabla_a T^{ab} = 0. \tag{172}$$

In [11], this is decomposed into four balance laws as

$$\nabla_a \left[T^{ab} (\partial_j)_b \right] = T^{ab} \nabla_{(a} (\partial_j)_{b)}, \tag{173}$$

$$\nabla_a \left(-T^{ab} n_b \right) = - T^{ab} \nabla_{(a} n_{b)}, \tag{174}$$

where n^a is the unit normal on the $t =$ const surfaces. The right-hand sides can be seen as a failure of stress-energy conservation to split into separate proper conservation laws for the energy and each momentum component, due to the failure of the three spatial coordinate basis vectors $(\partial_j)^a$ and the timelike unit normal vector n^a to be Killing. (This choice of the four basis vectors is merely conventional). In a 3+1 split, (173) and (174) become

$$\left(\alpha \sqrt{\gamma_x} T^0{}_j \right)_{,t} + \left(\alpha \sqrt{\gamma_x} T^i{}_j \right)_{,i} = \ldots, \tag{175}$$

$$\left(\alpha^2 \sqrt{\gamma_x} T^{00} \right)_{,t} + \left(\alpha^2 \sqrt{\gamma_x} T^{0i} \right)_{,i} = \ldots. \tag{176}$$

We now restrict to the elastic matter stress-energy tensor

$$T^{ab} = (e + p) u^a u^b + p g^{ab} + \pi^{ab}. \tag{177}$$

To insert this into (175) and (176), we need certain components of π^{ab}. From (76) and (10) we have

$$\pi_{00} = \pi_{ij} \hat{v}^i \hat{v}^j, \qquad \pi_{0i} = -\pi_{ij} \hat{v}^j. \tag{178}$$

Using the 3+1 decomposition of the metric, the components that we need in (175,176) are

$$\pi^{00} = \alpha^{-2}\pi_{ij}v^i v^j, \tag{179}$$
$$\pi^0{}_i = \alpha^{-1}\pi_{ij}v^j, \tag{180}$$
$$\pi^i{}_j = (\gamma^{ik} - \alpha^{-1}\beta^i v^k)\pi_{kj}, \tag{181}$$
$$\pi^{0i} = (\alpha^{-1}\gamma^{ij} - \alpha^{-2}\beta^i v^j)v^k\pi_{jk}. \tag{182}$$

From $g^{ab}\pi_{ab} = 0$, we have

$$v^i v^j \pi_{ij} = \gamma^{ij}\pi_{ij} =: \pi. \tag{183}$$

In numerical hydrodynamics, the conservation laws for the stress-energy are closed by the equation of state together with the explicit particle number conservation law

$$\nabla_a(nu^a) = 0. \tag{184}$$

As we have shown in Sec. 2.4, this evolution equation for n is equivalent to that for ${\psi^A}_i$ (with the hyperbolicity fix) even when the constraints are not obeyed. Therefore, where we write n below, either value could be used without changing the hyperbolicity. However, we shall test this numerically by obtaining a value n_ψ from ${\psi^A}_i$ and a value n_D from D, and using either the one or the other.

The conservation laws (173,174,184) can be written in the form

$$\left(\sqrt{\gamma_x}\mathcal{U}\right)_{,t} + \left(\alpha\sqrt{\gamma_x}\mathcal{F}^i\right)_{,i} = \mathcal{S}. \tag{185}$$

(Note the explicit insertion of $\sqrt{\gamma_x}$ and α, which is only a convention – we follow [11]). The conserved variables $\mathcal{U} = (D, S_i, \tau)$ are related to the primitive variables via

$$D = \alpha n u^0 = nW, \tag{186}$$
$$\begin{aligned} S_i &= \alpha T^0{}_i = nhW^2 v_i + \alpha\pi^0{}_i \\ &= nhW^2 v_i + \pi_{ij}v^j, \end{aligned} \tag{187}$$
$$\begin{aligned} \tau &= \alpha^2 T^{00} - D = nhW^2 - p + \alpha^2\pi^{00} - D \\ &= n(hW^2 - W) - (p - \pi), \end{aligned} \tag{188}$$

where we have defined the standard specific enthalpy

$$h := 1 + \epsilon + \frac{p}{n}. \tag{189}$$

The corresponding fluxes are

$$\mathcal{F}(D)^i = nu^i = n\alpha^{-1}W\hat{v}^i, \tag{190}$$
$$\mathcal{F}(S_j)^i = T^i{}_j = nhW^2\alpha^{-1}\hat{v}^i v_j + p\delta^i{}_j + \pi^i{}_j, \tag{191}$$
$$\begin{aligned} \mathcal{F}(\tau)^i &= \alpha T^{0i} - \mathcal{F}(D) \\ &= n(hW^2 - W)\alpha^{-1}\hat{v}^i + p\alpha^{-1}\beta^i + \alpha\pi^{0i} \\ &= n(hW^2 - W)\alpha^{-1}\hat{v}^i \\ &\quad + (p - \pi)\alpha^{-1}\beta^i + \gamma^{ij}\pi_{jk}v^k. \end{aligned} \tag{192}$$

The source terms are

$$\mathcal{S}(D) = 0, \tag{193}$$
$$\mathcal{S}(\tau) = \alpha^2\sqrt{\gamma_x}\left[T^{a0}\partial_a(\ln\alpha) - T^{ab}\Gamma^0{}_{ab}\right], \tag{194}$$
$$\mathcal{S}(S_j) = \alpha\sqrt{\gamma_x}T^{ab}\left[\partial_a g_{bj} - g_{cj}\Gamma^c{}_{ab}\right] = \frac{1}{2}\alpha\sqrt{\gamma_x}T^{ab}\partial_j g_{ab}. \tag{195}$$

Following [11], we have subtracted the rest energy from the total energy density in order to obtain the usual Newtonian energy conservation law in the Newtonian limit.

5.2. Conversion of conserved to primitive variables

In any numerical scheme, we frequently need to calculate the primitive variables n, v^i and ϵ from the related conserved variables D, S_i and τ, and hence further variables such as p and π_{ij} that appear in the fluxes. We assume that we have an equation of state that relates ϵ, n, s and I^α, and that we can use this to find the generalised forces p and f_α. For this relation to be unique for physical solutions (where ρ, ϵ are positive and the velocity sub-luminal) it should impose restrictions on both the equation of state and on the valid regions of parameter space. At present these precise restrictions are unknown, meaning the convergence of the methods discussed below can only be determined empirically. We also assume that g_{ab} is evolved using the Einstein equations, that k_{AB} is advected using (30) and that $\psi^A{}_i$ is evolved using the balance law (17). (Note that in the terminology of this subsection ψ^A_i is both a conserved and a primitive variable.)

The obvious difficulty is that to calculate π_{ij} from π_{AB}, we need v^i while π_{ij} is needed to extract v^i from S_j. We therefore need to proceed iteratively. We *guess* the primitive variables

$$p - \pi, \quad \pi_{ij} v^j. \tag{196}$$

From

$$\tau + D + (p - \pi) = nhW^2 \quad =: Z, \tag{197}$$

$$(S_i - \pi_{ik} v^k)(S_j - \pi_{jl} v^l)\gamma^{kl} = \; Z^2 v^2 \tag{198}$$

we obtain Z and v^2 and hence W from (A.15), followed by n_D from (186) and n_ψ from (38) (we compute both, but choose one value to use as n in the remainder of the calculation), v^i from (187) and h from (188). We now have a complete set of primitive matter variables, but these will not be consistent with the equation of state. We therefore now recompute p from the equation of state, compute g^{AB} from (50), and $\eta^A{}_B$ from k_{AB} and g^{AB}, and hence obtain $\pi^{1,2}_{AB}$ and $I^{1,2}$. We then compute π_{ab} from (76,77), using v^i and the equation of state. Hence we finally recompute $\pi_{ij} v^j$ and $p - \pi$. We then have four residuals giving the discrepancy (four numbers) between our original guesses (196) and the recomputed values, as a function of the four initial guesses. We can now use any standard root-finding method, such as a Newton solver, to find the solution (and hence the correct primitive values) to desired accuracy. (Note: this will converge only with a good initial guess, and a solution may not exist or be unique in general.)

Note that in the fluid limit we only need to guess p, and our scheme then reduces to the standard conserved-to-primitive conversion, requiring a root find in one variable [11].

6. Numerical tests

6.1. Description of the code

All of the variables in our computer code are 3-dimensional, but they are assumed to depend only on one or two spatial coordinates. The numerical methods employed are those in [22]. Briefly, the code uses a HRSC method with a third-order Runge-Kutta time evolution. In the reconstruction, standard slope limiting techniques, applied to the primitive variables are used – all results shown used van Leer's MC limiter ([23]).

The HLL approximate Riemann solver ([24]) is used to calculate the fluxes. The code can be run using either the relativistic or Newtonian set of governing equations.

The HLL flux is

$$\mathbf{f}_{i-\frac{1}{2}} = \frac{\mathbf{f}(\mathbf{q}^R_{i-1}) + \mathbf{f}(\mathbf{q}^L_i) + \bar{\lambda}_{\rm HLL}\left(\mathbf{q}^R_{i-1} - \mathbf{q}^L_i\right)}{2}, \tag{199}$$

where $\mathbf{q}^R_{i-1}$ and $\mathbf{q}^L_i$ are the right and left reconstructed vectors of conserved variables for the $(i-1)^{\rm th}$ and $i^{\rm th}$ cells, respectively, and $\bar{\lambda}_{\rm HLL}$ is an estimate of the absolute value of the largest coordinate characteristic speed. We set this either to $\max|\lambda|$ at one point (using the numerical calculation outlined in Sec. 4.8), to $\max|\lambda|$ over the whole grid, or to a constant. These three possibilities are in order of increasing efficiency and increasing dissipation but all can be made to work (possibly multiplying $\max|\lambda|$ by a constant fudge factor to get $\bar{\lambda}_{\rm HLL}$). Setting $\max|\lambda|$ over the whole grid allows us, in particular, to not update the calculation of the characteristic speeds within a complete Runge-Kutta step in the method of lines. Setting $\bar{\lambda}_{\rm HLL} = 1$ globally is sensible in highly relativistic situations (assuming the matter evolution is causal).

In two dimensions standard directional splitting techniques are used. Specifically, on our (logically) Cartesian grid we compute the appropriate one dimensional fluxes $\mathcal{F}^i$ required by equation (185) by sweeping through the grid lines one dimension at a time. The update terms are accumulated and applied simultaneously to minimize symmetry errors caused by the splitting.

We briefly note that the performance of the code has been compared to a relativistic hydrodynamics code by reducing the elasticity code explicitly to the hydrodynamic limit. As none of our codes have been optimized for performance, any comparisons will be approximate. Nevertheless, as the elasticity code is approximately 8 times slower than the hydrodynamic code on the same problem. We believe this is partly due to the greater number of evolved variables (19 instead of 5) and partly due to the fact that the conserved-to-primitive conversion requires a 4-dimensional instead of a 1-dimensional root find, and so there is no obvious way of reducing this ratio. (Adding spacetime evolution and adaptive mesh refinement to both hydro and elasticity would obviously reduce the overall ratio).

6.2. n_D versus n_ψ

As discussed in Sec. 5.2, the particle number density n can either be obtained from the conserved variable $\psi^A{}_i$ (or its inverse $F^i{}_A$ in the mixed framework), or from the conserved variable D. If we evolve D as a dynamical variable and use n_D to represent the primitive variable, we have one more variable than if we use n_ψ. However, we have shown in Sec. 2.4 the evolution equations for n_D and n_ψ are equivalent even if the constraints are not obeyed, and so we expect that both formulations have identical stability properties.

In fact, when these two evolutions are compared, the RMS relative error in the resulting data is small; we expect that this is finite-differencing error, as it converges away between first and second order. Hoewever, when n_ψ and n_D are compared for a single evolution where n_D is dynamical, the difference is of the order of round-off error rather than finite-differencing error; we suspect that this is an artifact of planar symmetry in those tests.

6.3. ψ versus F

A mixed framework using the inverse ${F^A}_i$ of the configuration gradient ${\psi^i}_A$ is outlined in Appendix D. For constraint satisfying initial data the results of the two frameworks should be the same. We have implemented both frameworks numerically and compared them. We find that the difference is on the order of the finite differencing error for constraint satisfying initial data, as expected.

Some of the tests given in [12] and [13] do not satisfy the constraints and so are unphysical – namely the second test in [12] and the fifth test in [13]. As the evolution of such data depends on the choice of constraint addition to the equations, we would expect it to depend on the framework used. Our numerical results obtained in the "mixed" framework (presented in Appendix D), which is that used in [12, 13], matches their numerical results for all tests. Our results using the Eulerian framework (presented in Sec. 2 and also used by [14, 21]) match only for the physical tests, where the initial data obey all constraints.

6.4. Newtonian Riemann tests

To validate our Newtonian code, and the Newtonian limit of our relativistic code, we have compared our results to two previously published studies ([12] and [13]). These results use the Newtonian theory and the mixed framework outlined in Appendix D.

Broadly the results obtained from our codes matched those shown in [12] and [13]. As an example, we show the results for the first test of [12] in Figs. 4–5, using the results of the Newtonian code. The precise initial data used is outlined in Appendix K. We see the seven waves expected for this solution; three left travelling rarefactions (the second is very small), a contact, two right travelling rarefactions (again the second is very small), and a fast shock. For clarity, the wave structure of the exact solution is shown in Fig. 3. All waves are captured with only minor under and overshoots, and the numerical solutions converge to the exact solution [25] with resolution, as seen by comparing Fig. 4 with Fig. 5.

Similar results are seen for all comparison tests. However, not all of the tests run robustly for all numerical methods possible within our code. An example is the sonic point test problem outlined in [13] (see in particular Figs. 5-7 there). At the contact discontinuity there is an unphysical "dip" in the density and a corresponding "jump" in the internal energy. This is the classical "wall-heating" effect seen by most numerical methods when strong rarefactions separate (e.g., on reflections from walls or the origin in spherical symmetry – see [26] for the classical case and [27] for a brief discussion of the relativistic case). This error can lead to unphysical states, and particular care is required with the choice of the Courant factor and $|\lambda|_{\rm HLL}$. The code fails if c_s^2 or n become (unphysically) negative (although the variant that sets $|\lambda|_{\rm HLL}$ a priori can limp on for a while with negative c_s^2). (Generally, there are two constraints on the Courant parameter and the value of $\lambda_{\rm HLL}$. The CFL (necessary) stability criterion requires $|\lambda|_{\rm max,global} < \Delta x/\Delta t$ while, depending on the time discretisation, $\lambda_{\rm HLL} < O(1)\Delta x/\Delta t$ to avoid an overdamping instability.)

Finally, we note that a direct and comprehensive comparison to the results of [13] is complicated by two issues. Firstly the units for the entropy appear inconsistent there, as detailed in Appendix K. Secondly we do not find agreement in the comparison of the pressure tensor p_{ij} (denoted σ there). As all other values and wave speeds match up well, and we have comprehensive quantitative agreement with the results of [12],

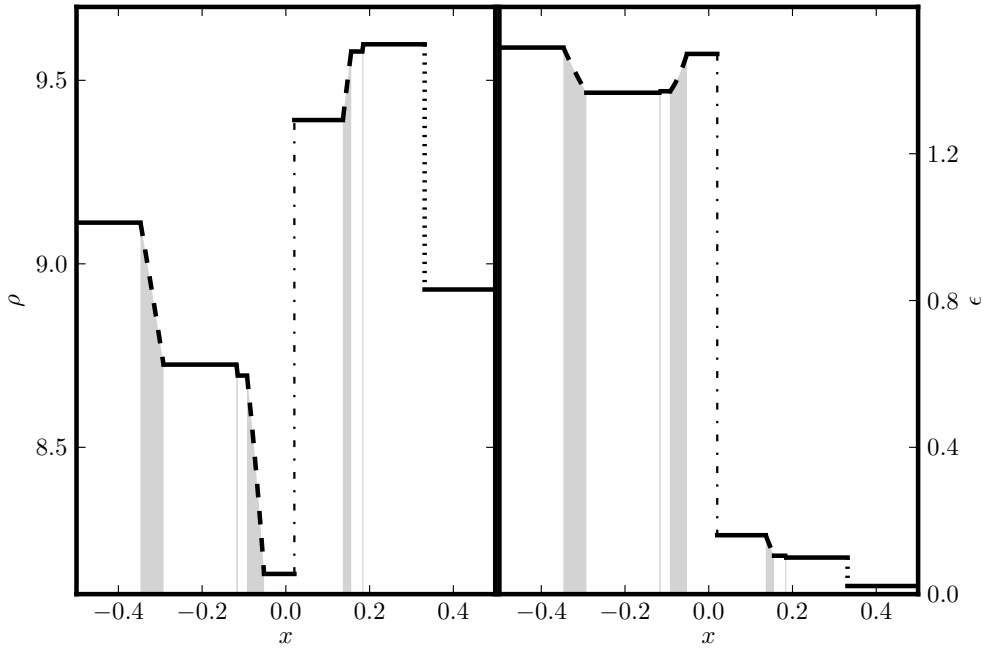

Figure 3: The density and specific internal energy in the first Newtonian Riemann test from [12] (from now on BDRT1), illustrating the seven waves possible in elastic matter. This is the exact solution, illustrating the wave structure in detail. The rarefactions – the 1, 2, 3, 5 and 6-waves – are given by the dashed lines and are shaded beneath to show the width of the fan. The contact – the linear 4-wave – is given by the dash-dotted line. The shock – the 7-wave – is given by the dotted line. It is clear that resolving some of the rarefaction waves will be difficult at moderate resolution.

we believe our results to be correct.

6.5. Newtonian limit vs Newtonian code

The code (both relativistic and Newtonian) uses geometric units where the speed of light is one. In particular, all velocities are of the form $v = \bar{v}/\bar{c}$ where v is a dimensionless velocity, $\bar{v}$ its value in conventional units and $\bar{c}$ the value of the speed of light in the same units. All parameters in the equation of state, such as ϵ and c_s^2, are treated analogously. There is no need to rescale rest mass and length, as long as units are used consistently.

Changing $\bar{c}$ while keeping $\bar{v}$ etc. fixed is a trivial scale invariance of the Newtonian equations and their solution, but in the relativistic equations decreasing $\bar{c}$ with $\bar{v}$ etc. fixed makes the same test problem more relativistic. We can use this to obtain an insight into the effects of (special) relativity, and to verify that our relativistic code has the correct Newtonian limit as $\bar{c} \to \infty$.

In Fig. 6 we show the results from the relativistic code run with a small range of values for $\bar{c}$. Only relatively small values of $\bar{c}$ are shown – $3, 5, 10$ and $20\,\mathrm{km\ s^{-1}}$, compared to a typical velocity in the (Newtonian) Riemann problem of $1\,\mathrm{km\ s^{-1}}$ –

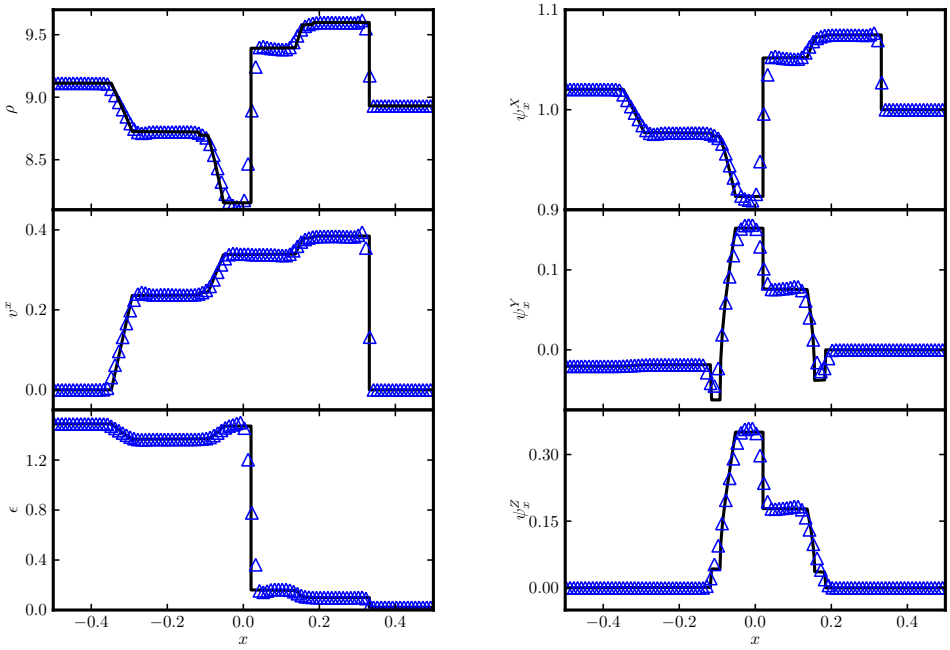

Figure 4: Numerical solution of the BDRT1 test at coordinate time $t = 0.06$. We show the results of our Newtonian code using 200 points (only 100 are plotted for clarity), with the exact solution given by the solid line. Density, specific internal energy and normal velocity are shown in the left panel and components of the configuration gradient in the right. Only minor under and overshoots are visible.

as for sufficiently large values of $\bar{c}$ the results are visually indistinguishable. We see that the results from the relativistic code are qualitatively similar, in terms of wave structure and accuracy, and approach the Newtonian results in the limit $\bar{c} \to \infty$.

6.6. Relativistic Riemann tests

In the genuinely relativistic limit we have tested our code against exact solutions constructed by solving a pre-determined wave structure. The explicit procedure is detailed in Appendix J and follows the method used in the Newtonian case outlined in [12], without constructing a full Riemann problem solver.

We have verified that the code behaves correctly for single shocks and rarefactions in the relativistic limit, and for some invented initial data sets that test a range of wave structures. As an example, we show in Figs. 8–9 the results for a four wave problem. For clarity, the wave structure of the exact solution is shown in Fig. 7. There are two left-going rarefactions (1 and 2-waves), one right-going rarefaction (a 6-wave) and a right going shock (7-wave). The central three waves – the nonlinear 3 and 5-waves and the contact – are all trivial. We note that some of the quantities change so rapidly across some rarefaction waves that they are only visually distinguishable from shocks at high magnification.

Even with the violent behaviour displayed across some waves in this four wave test, we find our code matching the exact solution well, with no unphysical oscillations

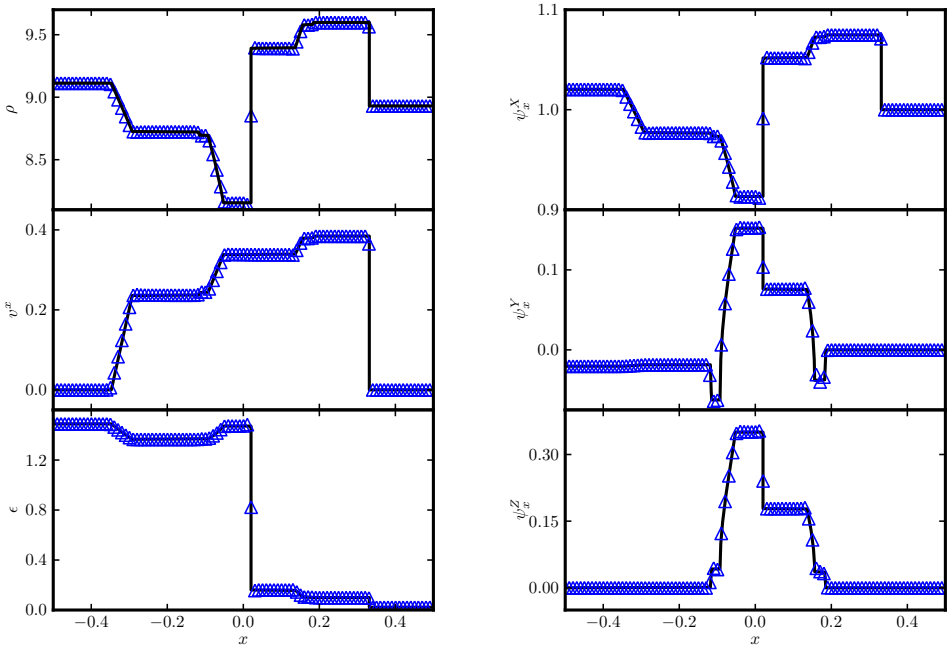

Figure 5: Numerical solution of the BDRT1 test at coordinate time $t = 0.06$. We show the results of our Newtonian code using 1000 points (only 100 are plotted for clarity), with the exact solution given by the solid line. Density, specific internal energy and normal velocity are shown in the left panel and components of the configuration gradient in the right. Only minor under and overshoots are visible. Comparing against the results in Fig. 4 we see convergence to the correct weak solution.

and only minor under and overshoots that converge away with resolution. There are the expected minor oscillations near the trivial waves, most noticeable near the contact, but again these converge with resolution.

6.7. Two-dimensional Riemann tests

The constraints are trivial if all variables depend only on one coordinate, for example when a Riemann problem is aligned with a Cartesian grid. As a first test of the behaviour in three dimensions and the role of the constraints, we have solved Riemann problems also at an arbitrary angle to a two-dimensional Cartesian grid. A method for carrying out such 2D simulations efficiently is described in Appendix F.

We put the initial discontinuity along lines $x/y = 0$ (our 1D tests), 1, 1/2 and 1/5, and use a cut along the x axis as an approximation to a line normal to the initial discontinuity. We compare this cut, suitably foreshortened, against the exact solution, in Fig. 10, with results similar to our 1D tests.

We have not implemented the "hyperbolicity fix" constraint additions for either the kinematic or dynamical evolution equations. In 1D the equations are symmetric hyperbolic anyway, as there are no constraints then, but in 2D our equations are not even strongly hyperbolic. Nevertheless, there is no sign of numerical instability in 2D. We have no explanation for this unexpected stability, but expect that constraint

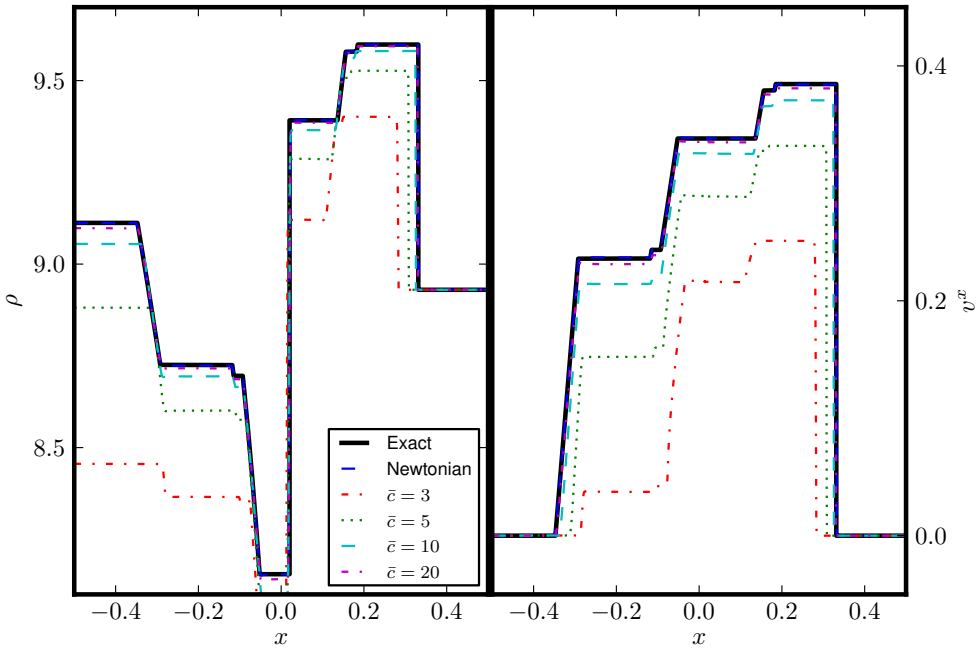

Figure 6: BDRT1 again, at coordinate time $t = 0.06$, but now run using the *relativistic* code with various values of $\bar{c}$, and compared against the Newtonian results. The results for ρ, v^x (appropriately scaled by $\bar{c}$) are representative of the behaviour of all quantities. We see that as $\bar{c}$ increases the Newtonian limit is approached. 10000 points were used in each case to ensure that we are at the continuum limit within the resolution of this plot.

addition will be necessary in other tests in the future.

6.8. Two-dimensional rotor tests

To study a problem with nontrivial dependence on two Cartesian coordinates we consider a test suggested by [33]. The initial data, detailed in Appendix K, represents an elastic rotor problem, where an inner rotating bearing is instantaneously welded to the non-rotating exterior, causing the rotor to slow and propagating elastic waves through the material. This is a cylindrically symmetric problem simulated in Cartesian coordinates. In all cases the rotor has coordinate radius 0.1, whilst the exterior is at rest. In all numerical experiments shown here 400^2 points were used.

Results for the Newtonian case are shown at representative coordinate times in Fig. 11. These should be compared to the results shown by Dumbser et al. in [33]. The results in the literature use a considerably more accurate numerical method, which is both higher order and uses finite elements better adapted to the symmetry of the problem. Despite this, we see qualitative agreement in the waves emitted during the evolution of the problem.

Results for the relativistic case are shown at representative coordinate times in Fig. 12. Again we see qualitative agreement in the emitted wave structure, despite the differences in the models.

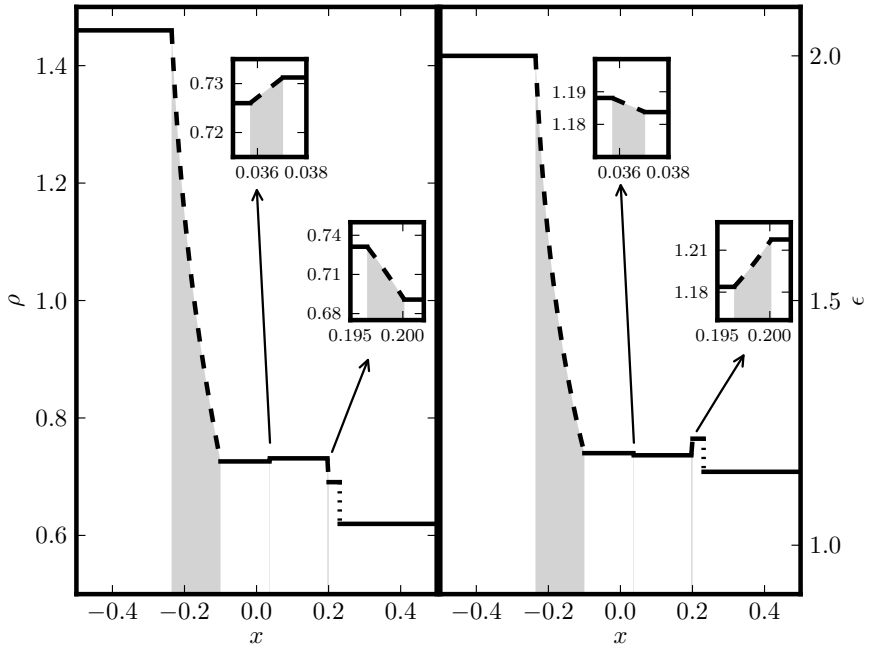

Figure 7: The density and specific internal energy ϵ for the relativistic 4-wave test at coordinate time $t = 0.25$. This is the exact solution, illustrating the wave structure in detail. The rarefactions – the 1, 2, and 6-waves – are given by the dashed lines and are shaded beneath to show the width of the fan. The very narrow 2 and 6-waves are shown in detail in the insets. The contact – the linear 4-wave – is trivial. The shock – the 7-wave – is given by the dotted line. It is clear that resolving some of the rarefaction waves will be difficult at moderate resolution.

6.9. Tests in two-dimensional curvilinear coordinates

To test the functioning of the code with a metric other than the Minkowski metric in Cartesian coordinates, we have implemented several tests in Minkowski cylindrical coordinates. We describe the details of implementing this cylindrical grid in Appendix G. We use two different Newtonian tests to demonstrate that the code can handle curvilinear coordinates: a Riemann problem (BDRT1, [12]) and an off-axis ring rotor, with initial data described in further detail in Appendix K. The symmetry of each of these tests is obscured on the cylindrical grid; this allows us to compare the two-dimensional cylindrical evolutions to one-dimensional evolutions that take advantage of the symmetry of the physical systems (cylindrical symmetry for the ring rotor and planar symmetry for the Riemann test), giving us confidence that the code is self-consistent.

The results of the off-axis ring rotor evolved on the two-dimensional cylindrical grid show good agreement with both the results of a one-dimensional evolution of an axisymmetric ring rotor, suitably shifted, as well as the results of a two-dimensional Cartesian evolution of the same ring rotor. As the resolution is increased, the results of the 2D cylindrical evolution approach those of the 1D evolution. Fig. 13a shows a pseudocolour plot of the density with a vector plot of the velocity at coordinate time

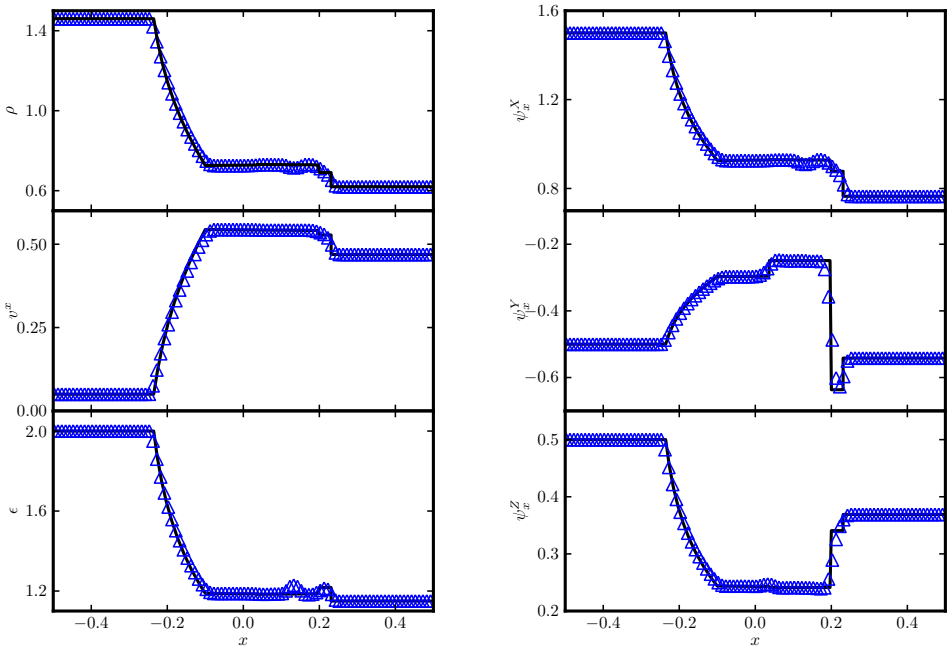

Figure 8: Numerical solution of the relativistic 4-wave test at coordinate time $t = 0.25$. Density, specific internal energy and normal velocity are shown in the left panel, and components of the configuration gradient in the right. The 4 wave structure (two left-going rarefactions, one right-going rarefaction and one right going shock) is most clearly seen in the plot of $\psi^Y{}_x$. The solution is computed using 200 points but only 100 are plotted for clarity. We see that all waves are captured well and with only minor under and overshoots, most visible for the second rarefaction wave in quantities such as ϵ.

$t = 0.0095$. The initial velocity within the rotating ring is a rigid rotation, while the outer regions are static. In the density plot, waves can be seen propagating away from both edges of the ring.

The Riemann problem results on the 2D cylindrical grid also approach the published exact solution [12] with increased resolution. Fig. 13b shows a pseudocolour plot of the density for the Riemann problem on a 2D cylindrical grid at coordinate time $t = 0.02$. Waves can be seen propagating away from the initial discontinuity. The boundary conditions are not consistent with the symmetries of the initial data, giving rise to error at the boundaries; this is discussed further in Appendix G.

7. Conclusions

We have presented a framework that can be used for simulating nonlinear elasticity in numerical relativity, and checked its viability in numerical tests. The framework can be directly related to existing approaches and is a first step towards the simulation of neutron star crusts.

Our numerical simulations implementing the Newtonian limit of the equations

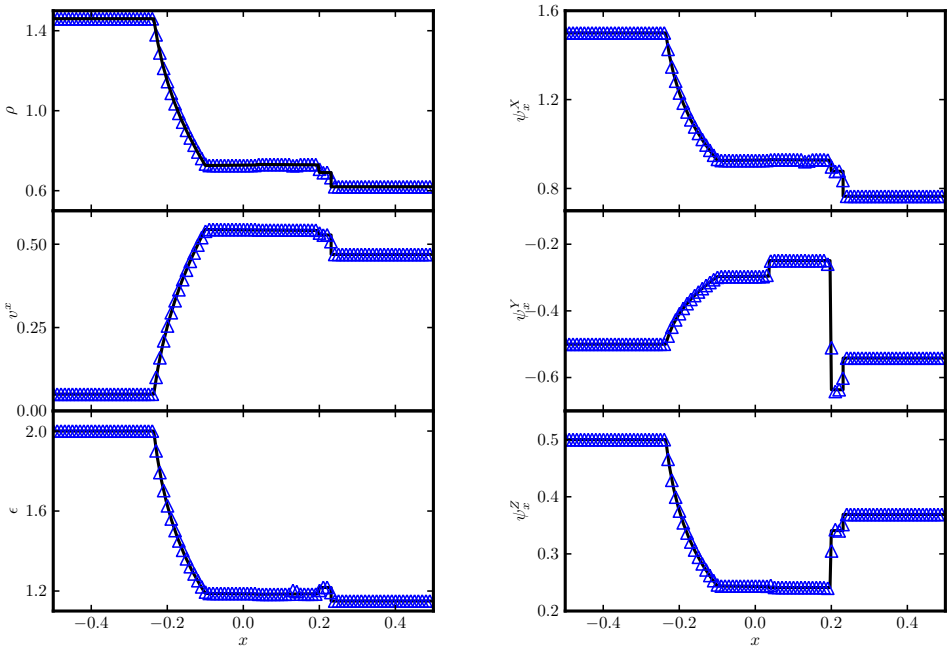

Figure 9: Numerical solution of the relativistic 4-wave test at coordinate time $t = 0.25$. Density, specific internal energy and normal velocity are shown in the left panel, and components of the configuration gradient in the right. The solution is computed using 1000 points but only 100 are plotted for clarity. We see that all waves are captured well and with only minor under and overshoots, and comparing to Fig. 8 we see the expected convergence.

match those in the Newtonian literature, and so does our *relativistic* code when effectively running in the Newtonian limit. While our fully relativistic tests are limited to Minkowski spacetime in Cartesian coordinates, they do test special relativistic effects (Lorentz factor $W \gg 1$). From experience with relativistic fluid codes, we do not expect substantial difficulties in the generalisation to a fixed curved spacetime in regular coordinates, or, as spacetime and matter couple only through lower-order terms, to a dynamical spacetime. We give two examples of Newtonian simulations in cylindrical coordinates as an indication that the addition of source terms arising from curvilinear coordinates and/or curved spacetimes does not give rise to any problems.

The equations in first order form consist of three groups: evolution equations for a *configuration gradient* ${\psi^A}_i$, auxiliary constraints ${\psi^A}_{[i,j]} = 0$ for these variables due to the fact that ${\psi^A}_i = \partial\chi^A/\partial x^i$ for an implicit underlying *configuration* χ^A, and energy-momentum conservation laws.

The first two groups are purely kinematical in the sense that they are independent of the geometry of both spacetime and matter space, and hence are the same in Newtonian and relativistic elasticity. However, from a spacetime point both the evolution equations and constraints naturally arise as components of a single spacetime constraint ${\psi^A}_{[a,b]} = 0$. (In fact, without the benefit of this point of view, some of the constraints seem to have been systematically overlooked in the Newtonian literature,

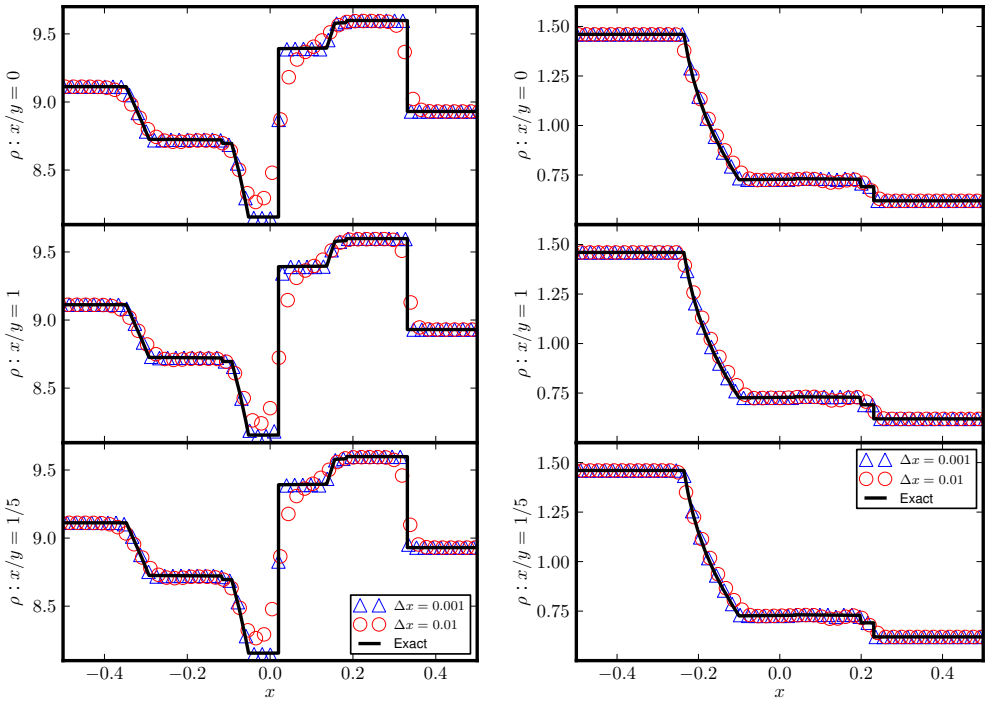

Figure 10: Results for the BDRT1 Riemann test at coordinate time $t = 0.06$ (left panel) and relativistic 4 wave test at coordinate time $t = 0.25$ (right panel), calculated on a two-dimensional grid for three different angles between the initial discontinuity and the grid, each at two resolutions. The initial discontinuity was placed on the line given alongside each plot. In order to compare the results to the exact solution, a slice through the two-dimensional grid is taken along the x axis (as an approximation to a line normal to the waves), and x is scaled to correspond to distance perpendicular to the initial discontinuity. The spatial resolution is independent of the angle of the initial discontinuity, and the snapshot is always taken at the same time, for all angles. The relativistic code is used in both cases (in the Newtonian limit for the BDRT test). The high-resolution results were produced using $\Delta x = \Delta y = 0.001$. (The effective resolution in the relevant direction, normal to the initial discontinuity, is lower (by a factor of $\sqrt{2}$ in the worst case where the initial discontinuity is on the grid diagonal)). The low-resolution version was produced using $\Delta x = \Delta y = 0.01$. (For clarity, only 1 in 2 or 1 in 20 points are plotted for the $x/y = 0$ and $x/y = 1/5$ cases, while 1 in 3 or 1 in 28 points are plotted for $x/y = 1$.) All evolutions look similar, with the results approaching the exact solution as the resolution is increased.

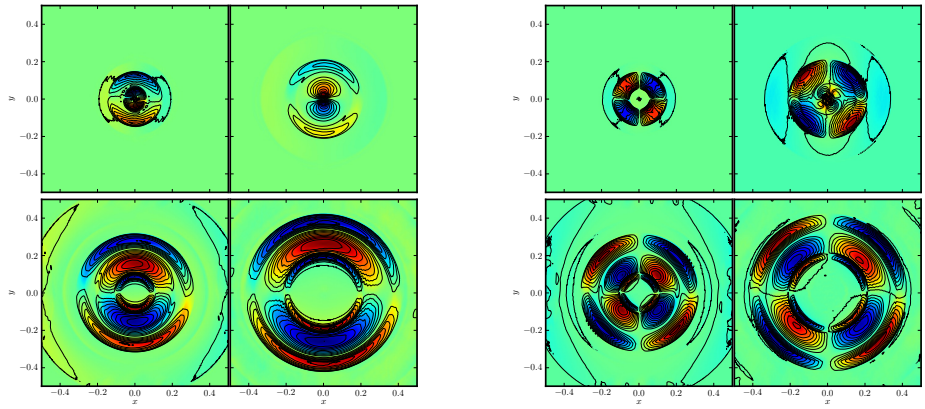

Figure 11: Newtonian rotor test, following [33]. An initially rotating central cylinder is slowed by the interaction with the exterior, which is initially at rest. The figures in the left panel show ρv^x whilst those in the right show $\rho F^y{}_Y$, at coordinate times $t = 0.02, 0.05, 0.1$ and 0.15. The results qualitatively match those in Fig. 24 of [33].

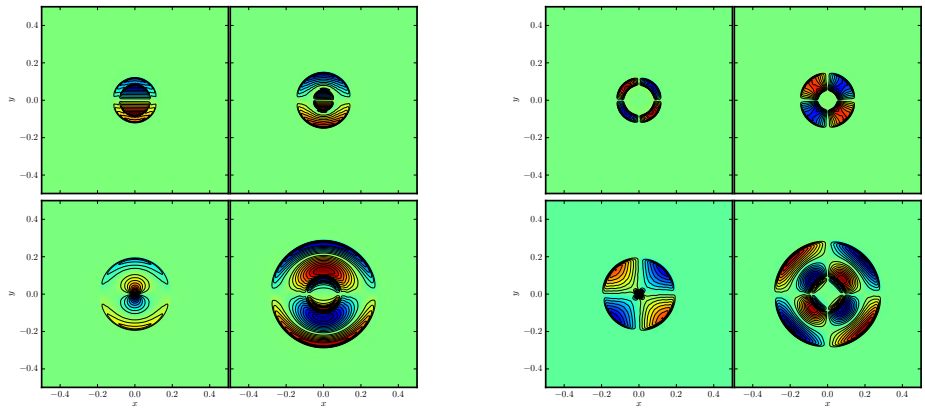

Figure 12: Relativistic rotor test, to be compared with the Newtonian results in Fig. 11. An initially rotating central cylinder is slowed by the interaction with the exterior, which is initially at rest. These figures in the left panel show ρv^x whilst those in the right show $\rho F^y{}_Y$, at coordinate times $t = 0.02, 0.05, 0.1$ and 0.2. The emitted waves are qualitatively similar to the Newtonian results.

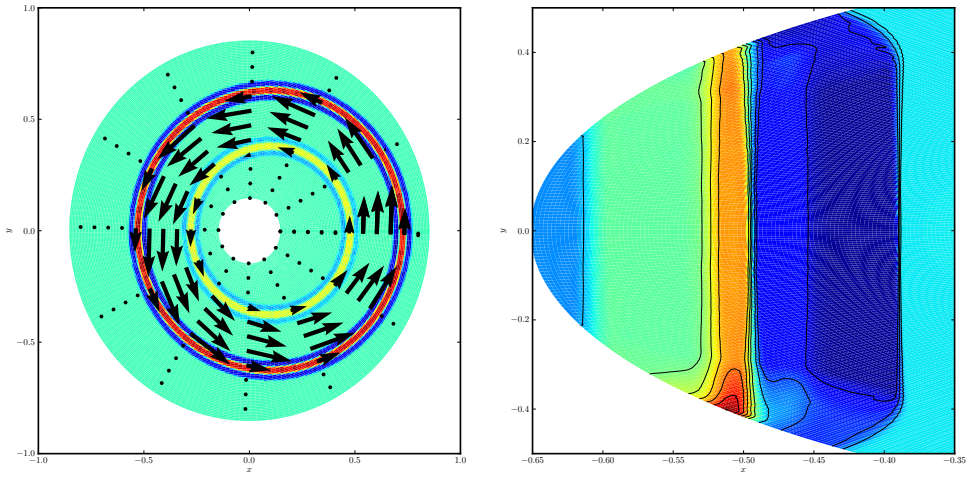

(a) (b)

Figure 13: Tests on a two-dimensional cylindrical grid. Fig. 13a shows a pseudocolour density plot and velocity vector plot for a ring rotor at coordinate time $t = 0.0095$. The initial velocity within the rotating region is a rigid rotation, while the outer and inner regions are static. The numerical domain is an annulus, with the origin of cylindrical coordinates cut out. In the density plot, waves are visible propagating away from the initial discontinuity. In an equivalent shear test in planar symmetry with a static inner and outer region and a central region with non-zero velocity parallel to the initial discontinuities, one would expect the Riemann problem solutions around the two discontinuities to be symmetrical; the asymmetry visible in the ring rotor version is due to the curvature of the discontinuity and centrifugal forces. Fig. 13b shows a pseudocolour density plot of the BDRT1 Riemann test at coordinate time $t = 0.02$. Plane waves can be seen propagating away from the initial discontinuity at $x = -0.5$. Only a part of the annular numerical domain is shown. In the plot, the effect of the incorrect boundary conditions can also be seen as the solution near the boundaries is incorrect – this is seen also in Fig. 14.

giving rise to the numerical solution of unphysical Riemann problems in [13, 12].)

Energy-momentum conservation is due to time and space translation invariance, and this fixes their correct weak form [11]. The weak form of the kinematical equations appears to have been assumed *ad hoc* in the Newtonian literature. Here we have rigorously derived it from the absence of dislocations in the elastic matter.

There are two rather different frameworks in the Newtonian literature. One of these [15, 14, 21] is fully Eulerian and arises naturally as the Newtonian limit of our relativistic framework. The other [16, 17, 18] mixes Eulerian and Lagrangian points of view and gives rise to more complicated evolution equations. For completeness, we have proved that the two frameworks are equivalent in their *weak* form, and hence that the weak form of the second framework is also correct. This is borne out by our numerical tests, which agree for both frameworks (if and only if the initial data obey the constraints).

The *dynamical* equations of our framework can be related to the standard Valencia formalism for relativistic hydrodynamics. Although, as noted in Sec. 2, the fluid

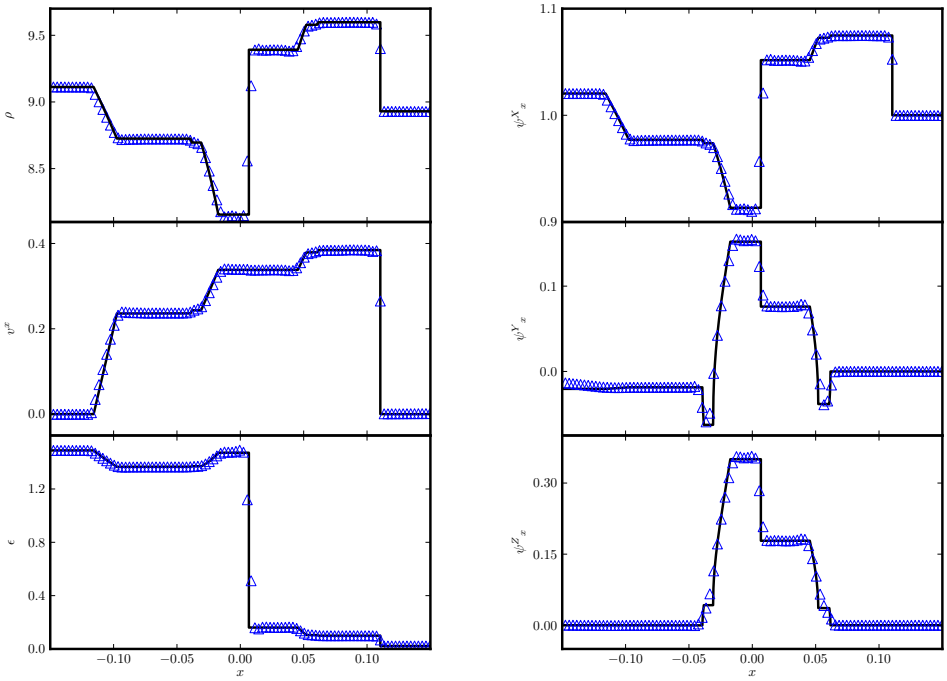

Figure 14: One-dimensional slice of BDRT1 test at coordinate time $t = 0.02$ evolved on a two-dimensional cylindrical grid. Here the numerical domain was an annulus with 300 points in the r direction and 601 in the angular direction; only 1 out of every 3 points is plotted here for clarity. The results have also been transformed from cylindrical coordinates, which are used for evolution, to Cartesian coordinates, as described in Appendix G. In addition, while the transformed version of the BDRT1 intial data was used (see Appendix K), the matter-space indices have been transformed back to the coordinate system of the original BDRT1 test for comparison with the exact solution presented in [12]. The results using a two-dimensional cylindrical grid visually match well with the exact solution; the only notable feature is that the effect of the incorrect boundary conditions can be seen near the left edge of the plot for $\psi^Y{}_x$.

limit is singular, the system presented takes the form of the Valencia equations with additional terms. We also note that steps within the numerical code, such as the conversion to primitive variables outlined in Sec. 5.2, tend towards standard algorithms in the fluid limit.

Using the methods of [10], we have shown that our framework can be made symmetric hyperbolic, at least in a neighbourhood of the unsheared state of the matter, if certain linear combinations of the auxiliary constraints are added as source terms to the conservation laws. We have also shown that if constraints are added only to the kinematic evolution equations, bringing them into the form (17) (the "hyperbolicity fix"), but not to $\nabla_a T^{ab} = 0$, the resulting first-order system is strongly hyperbolic but not symmetric hyperbolic.

The latter is precisely the situation in the Newtonian literature, and so the

Newtonian limit of our result shows that the equations given there [18, 14] are only strongly hyperbolic but could be made symmetric hyperbolic by a simple constraint addition.

There remain two outstanding issues before this framework can be used in a fully nonlinear GR simulation of a neutron star. The first is the issue of the integrability constraints in higher dimensional simulations. In the Newtonian literature it is clear that the hyperbolicity fix included here is required to obtain stable evolutions. However, there is no agreement as to the impact of constraint violations on the *accuracy* of the simulations. In analogy with MHD simulations where the $\nabla \cdot \mathbf{B} = 0$ constraint is crucial for accuracy, we might expect that methods for reducing constraint violations (such as the parabolic damping term used by [28] – similar to the Powell method for MHD), or alternatively a discretisation that maintains a discrete version of the constraints along the lines of Appendix E, will be important.

Secondly, to be useful for simulating a neutron star, we must couple the elastic crust to the fluid interior and vacuum exterior. A framework for the nonlinear simulation of multiple matter models separated by sharp interfaces in GR was studied in [22], but only for fluid-fluid interactions. This model built on standard Newtonian methods which have themselves been extended to deal with solid-fluid interactions; we expect that these methods will extend to relativity as well.

Acknowledgments

We are grateful to Philip Barton for discussions and for the numerical data corresponding to the exact solutions of the problems in [12]. We are also grateful to Lars Samuelsson, Bobby Beig, Lars Andersson and members of the Southampton General Relativity Group for discussions relating to this work.

Appendix A. 3+1 split of spacetime

For reference, we assemble some standard formulas. In 3+1 numerical relativity, the spacetime metric g_{ab} is split into a spatial metric γ_{ij} with inverse γ^{ij}, a lapse α and shift β^i, as

$$g_{00} = -\alpha^2 + \beta_i\beta^i, \quad g_{0i} = \beta_i, \quad g_{ij} = \gamma_{ij}, \tag{A.1}$$

where we define indices on β^i to be moved implicitly with γ_{ij}. The (absolute value of the) determinant of the 4-metric is given by

$$g_x = \alpha^2\gamma_x \tag{A.2}$$

and hence the volume forms on M^3 and M^4 are related by

$$\epsilon^{0ijk} = \alpha\epsilon^{ijk}. \tag{A.3}$$

The inverse 4-metric is

$$g^{00} = -\alpha^{-2}, \quad g^{0i} = \alpha^{-2}\beta^i, \quad g^{ij} = \gamma^{ij} - \alpha^{-2}\beta^i\beta^j. \tag{A.4}$$

The covector normal to the surfaces of constant t has components

$$n_0 = -\alpha, \qquad n_i = 0, \tag{A.5}$$

and hence

$$n^0 = \alpha^{-1}, \qquad n^i = -\alpha^{-1}\beta^i. \tag{A.6}$$

Hence the projector into the surfaces of constant t

$$\gamma_{ab} := g_{ab} + n_a n_b \tag{A.7}$$

has components

$$\gamma_{00} = \beta_i \beta^i, \quad \gamma_{0i} = \beta_i, \quad \gamma_{ij} = \gamma_{ij}, \tag{A.8}$$

and

$$\gamma^{00} = 0, \quad \gamma^{0i} = 0, \quad \gamma^{ij} = \gamma^{ij}. \tag{A.9}$$

We define the convective derivative to be the derivative along the 4-velocity,

$$u^a \frac{\partial}{\partial x^a} \propto \frac{\partial}{\partial t} + \hat{v}^i \frac{\partial}{\partial x^i}. \tag{A.10}$$

The factor of proportionality is given by the normalisation condition

$$u^a u^b g_{ab} = -1. \tag{A.11}$$

We find

$$u^a = (u^t, u^i) = \alpha^{-1} W (1, \hat{v}^i), \tag{A.12}$$

$$u_a = (u_t, u_i) = W(-\alpha + v_j \beta^j, v_i), \tag{A.13}$$

where

$$\hat{v}^i := \alpha v^i - \beta^i, \tag{A.14}$$

$$W := \left(1 - v_i v^i\right)^{-1/2}, \tag{A.15}$$

and where we define the indices on v^i to be moved implicitly with γ_{ij}. The scalar

$$-u^a n_a = W \tag{A.16}$$

gives the Lorentz factor of the relative velocity between the matter and the time slices.

Appendix B. Definitions of hyperbolicity

We summarise some standard definitions [10, 30] in our notation. Let w^α be a vector of variables obeying the system of first-order partial differential equations

$$P_{\alpha\beta}{}^c w^\beta_{,c} + \text{l.o.} = 0, \tag{B.1}$$

where l.o. stands for lower order terms. Obviously the index $\alpha = 1 \ldots n$ labelling the equations needs to take as many values as the index β labelling the variables.

Assume, however, that α is an index of the same type as β and that $P_{\alpha\beta}{}^c = P_{\beta\alpha}{}^c$. Then we have a conserved current (up to lower order terms) in the sense that

$$J^c{}_{,c} = \text{l.o.}, \qquad J^c := P_{\alpha\beta}{}^c w^\alpha w^\beta. \tag{B.2}$$

If furthermore there exists a covector t_c with the property that

$$E(w, w) := t_c J^c = t_c P_{\alpha\beta}{}^c w^\alpha w^\beta \tag{B.3}$$

is positive definite, called a subcharacterisic vector, then the system is called symmetric hyperbolic. (In a relativistic context we expect t_c to be timelike.) E allows us to estimate an L^2 norm called an energy norm of the solution in terms of the initial data and boundary data.

A characteristic direction is a covector k_c such that

$$\det k_c P_{\alpha\beta}{}^c = 0 \tag{B.4}$$

and the corresponding characteristic variable w^α is the non-zero vector obeying

$$k_c P_{\alpha\beta}{}^c w^\beta = 0. \tag{B.5}$$

This means that a plane wave with amplitude w^β and wave number k_c is a solution of the principal part. For a causal system in relativity, influence cannot travel faster than light, and so k_c must be spacelike or null.

For a second-order system

$$P_{\alpha\beta}{}^{cd} w^\beta_{,cd} + \text{l.o.} = 0 \tag{B.6}$$

the equivalent definition of a characteristic direction and variable is

$$k_c k_d P_{\alpha\beta}{}^{cd} w^\beta = 0, \tag{B.7}$$

and it has the same interpretation as a plane wave solution of the principal part.

It is often useful to decompose the characteristic equation with respect to a preferred time direction. Let

$$k_a = \lambda n_a - e_a \tag{B.8}$$

where n_a is a unit timelike covector and e_a a unit spacelike covector normal to n_a. λ is called the characteristic velocity (relative to n_a, in the direction e_a) of the characteristic variable w^α. k_a is normal to the characteristic plane spanned by the vectors

$$v^a = n^a + \lambda e^a + s^a \tag{B.9}$$

where s^a is any vector normal to both n_a and e_a (so that $k_a v^a = 0$). The relative speed between n^a and v^a (calculated from $n^a v_a/|n||v|$) is $\sqrt{\lambda^2 + s^a s_a} \geq \lambda$. The disturbance itself moves along $n^a + \lambda e^a$, that is in the direction e^a with speed λ as measured by n^a observers. One natural choice of n_a is the unit normal to the surfaces of constant time t, and the resulting values of λ are used in our numerical scheme. By contrast, choosing $n_a = u_a$ gives the speed of the disturbances relative to the matter, which are simpler to compute.

To make contact with non-relativistic concepts of hyperbolicity, we rewrite the first order characteristic equation (B.4) as

$$\mathcal{P}_e w = \lambda w, \qquad \mathcal{P}_e := (n_a P^a)^{-1}(e_b P^b) \tag{B.10}$$

where we have not written the Greek indices for simplicity. (If n_a is subcharacteristic, $n_a P^a$ is positive definite and so has an inverse.) The system is then called weakly hyperbolic with respect to the time direction n_a if $\mathcal{P}_e$ has real eigenvalues λ for all unit vectors e_a normal to n_a. It is called strongly hyperbolic if furthermore $\mathcal{P}_e$ has a basis of real eigenvectors that depends continuously on e_a. It is called symmetric hyperbolic if $\mathcal{P}_e$ is symmetric. As a real symmetric matrix is always diagonalisable with real eigenvalues, symmetric hyperbolicity implies strong hyperbolicity. More generally, the system is called symmetric hyperbolic, or symmetrisable, if there exists a symmetriser, a positive definite symmetric matrix $\mathcal{H}$ independent of e^a such that $\mathcal{P}_e \mathcal{H}$ is symmetric. In this case $E = \mathcal{H}_{\alpha\beta} w^\alpha w^\beta$.

Appendix C. The Newtonian limit

We obtain the limit of Newtonian motion in the absence of gravity in two steps. In the first step, we let the spacetime go to Minkowski spacetime in adapted coordinates,

$$ds^2 = -dt^2 + \gamma_{ij}\, dx^i\, dx^j, \tag{C.1}$$

where γ_{ij} is flat and independent of t, but x^i could still be curvilinear coordinates. Hence

$$\hat{v}^i = v^i, \tag{C.2}$$

and the advection equation (30) becomes

$$(\partial_t + v^i\partial_i)k_{AB} = 0. \tag{C.3}$$

In the second step, we use dimensional analysis of the special relativistic equations of motion to insert a parameter c representing the speed of light, as follows:

$$n, \tag{C.4}$$
$$c^{-1}v^i, \tag{C.5}$$
$$c^{-2}\epsilon, \quad c^{-2}p, \quad c^{-2}\pi_{ij}, \tag{C.6}$$
$$c^{-3}\pi_{0i}, \quad c^{-4}\pi_{00}, \tag{C.7}$$

for the primitive variables, and

$$D, \quad c^{-1}S_i, \quad c^{-2}\tau, \tag{C.8}$$
$$c^{-1}\mathcal{F}(D)^i, \quad c^{-2}\mathcal{F}(S_j)^i, \quad c^{-3}\mathcal{F}(\tau)^i, \tag{C.9}$$

for the conserved variables. We then take the limit $c \to \infty$ of the relevant equations for Minkowski spacetime. In this limit,

$$W = 1, \tag{C.10}$$
$$u^a = n^a, \tag{C.11}$$
$$h_{ab} = \gamma_{ab}, \tag{C.12}$$
$$\psi^A{}_t = 0, \tag{C.13}$$
$$\pi = \gamma^{ij}\pi_{ij} = 0, \tag{C.14}$$
$$D = n, \tag{C.15}$$
$$S_i = nv_i, \tag{C.16}$$
$$\tau = n(v^2/2 + \epsilon), \tag{C.17}$$
$$\mathcal{F}(D)^i = nv^i, \tag{C.18}$$
$$\mathcal{F}(S_j)^i = nv_jv^i + p\delta^i{}_j + \pi^i{}_j, \tag{C.19}$$
$$\mathcal{F}(\tau)^i = n(v^2/2 + \epsilon)v^i + pv^i + \pi^i{}_jv^j, \tag{C.20}$$
$$\mathcal{S}(D) = 0, \tag{C.21}$$
$$\mathcal{S}(\tau) = 0, \tag{C.22}$$
$$\mathcal{S}(S_j) = \frac{1}{2}\sqrt{\gamma_x}T^{ik}\partial_j\gamma_{ik}. \tag{C.23}$$

where v^i and π_{ij} are now the Newtonian velocity and stress tensor, and their indices are moved implicitly with the metric γ_{ij} of Euclidean space. Instead of requiring p, f_1 and f_2 as functions of h (the relativistic enthalphy, which includes the rest mass energy) and n, we need them as functions of ϵ and n. The reconstruction of n, v_i and ϵ from D, S_i and τ becomes explicit for the equations of state we consider.

Appendix D. The mixed framework

Variables In the alternative Newtonian framework of [18, 17], the deformation is given by a map from a 3-dimensional matter space and time to 3-dimensional space

$$R \times X_3 \to M_3, \tag{D.1}$$

$$(t, \xi^A) \ \mapsto x^i \tag{D.2}$$

with derivatives

$$F^i{}_A := \frac{\partial x^i}{\partial \xi^A}, \qquad \hat{v}^i := \left.\frac{\partial x^i}{\partial t}\right|_{\xi^A = \text{const}}, \tag{D.3}$$

where $F^i{}_A$ is the 3×3 matrix inverse of $\psi^A{}_i$. We shall call this the mixed framework, as the dependent variables are Lagrangian, but the coordinates are still (t, x^i). (A purely Lagrangian framework also exists, but is not relevant for us because we are interested in finite volume methods for weak solutions.)

For the purpose of a systematic derivation of the kinematic equations, and a comparison with the Eulerian framework, we add a time coordinate τ to matter space, which now has coordinates $\xi^\alpha = (\tau, \xi^A)$. To make this extension trivial, we then fix $\tau = t$. Note that

$$\frac{\partial}{\partial \tau} = \frac{\partial}{\partial t} + \hat{v}^i \frac{\partial}{\partial x^i} \tag{D.4}$$

is then the usual convective derivative. This extension gives us the extended derivatives

$$\tilde{F}^a{}_\alpha = \begin{pmatrix} 1 & 0_A \\ \hat{v}^i & F^i{}_A \end{pmatrix}, \tag{D.5}$$

$$\tilde{\psi}^\alpha{}_a = \begin{pmatrix} 1 & 0_i \\ \psi^A{}_t & \psi^A{}_i \end{pmatrix}, \tag{D.6}$$

which are now 4×4 matrix inverses of one another, assuming (10).

Kinematic equations We derive the evolution equations and constraints in the mixed framework by working in the 4-dimensional notation at first. The integrability condition

$${}^{(1)}\tilde{\mathcal{C}}^a{}_{\alpha\beta} := \tilde{F}^a{}_{[\alpha,\beta]} = 0 \tag{D.7}$$

can be written as the commutator of the vector fields ∂_α and ∂_β pushed forward with $\tilde{F}^a{}_\alpha$ to spacetime,

$${}^{(2)}\tilde{\mathcal{C}}^a{}_{\alpha\beta} := \tilde{F}^a{}_{[\alpha}\tilde{F}^b{}_{\beta],a} = \frac{1}{2}[\partial_\alpha, \partial_\beta]^b = 0. \tag{D.8}$$

We define the determinant

$$\tilde{F}_{x\xi} := \frac{1}{4!}\delta_{abcd}\delta^{\alpha\beta\gamma\delta}\tilde{F}^a{}_\alpha\tilde{F}^b{}_\beta\tilde{F}^c{}_\gamma\tilde{F}^d{}_\delta, \tag{D.9}$$

where the suffixes indicate that this depends explicitly on the coordinates x^a and ξ^α. With $\tilde{\psi}$ the inverse of $\tilde{F}$, we have the variation-of-determinant rule

$$\frac{\delta \tilde{F}_{x\xi}}{\delta \tilde{F}^a{}_\alpha} = \tilde{F}_{x\xi}\ \tilde{\psi}^\alpha{}_a. \tag{D.10}$$

As δ_{abcd} and $\delta_{\alpha\beta\gamma\delta}$ are constant, we therefore have

$$\tilde{F}_{x\xi,b} = \tilde{F}_{x\xi}\ \tilde{\psi}^\alpha{}_a\ \tilde{F}^a{}_{\alpha,b}. \tag{D.11}$$

From (D.11) and (D.7), we find that

$$\tilde{\mathcal{C}}_\alpha := \left(\tilde{F}^{-1}_{x\xi}\tilde{F}^a{}_\alpha\right)_{,a} = 0, \tag{D.12}$$

while combining (D.8) and (D.12) we obtain

$${}^{(3)}\tilde{\mathcal{C}}^b{}_{\alpha\beta} := 2\left(\tilde{F}^{-1}_{x\xi}\tilde{F}^a{}_{[\alpha}\tilde{F}^b{}_{\beta]}\right)_{,a} = 0. \tag{D.13}$$

Developing (D.5) into its first row, we find

$$\tilde{F}_{x\xi} = \frac{1}{3!}\delta_{ijk}\,\delta^{ABC}F^i{}_A F^j{}_B F^k{}_C =: F_{x\xi} \tag{D.14}$$

Hence we obtain the 3+1 split of the 4-dimensional constraints into evolution equations and constraints:

$$\mathcal{C}_A \quad := \tilde{\mathcal{C}}_A = \left(F^{-1}_{x\xi}F^i{}_A\right)_{,i} = 0, \tag{D.15}$$

$$\mathcal{E} \quad := \tilde{\mathcal{C}}_\tau = \left(F^{-1}_{x\xi}\right)_{,t} + \left(\hat{v}^i F^{-1}_{x\xi}\right)_{,i} = 0, \tag{D.16}$$

$$\mathcal{C}^i{}_{AB} := -{}^{(3)}\tilde{\mathcal{C}}^i{}_{AB} = \left(F^{-1}_{x\xi}F^i{}_{[A}F^j{}_{B]}\right)_{,j} = 0, \tag{D.17}$$

$$\mathcal{E}^i{}_A \quad := -{}^{(3)}\tilde{\mathcal{C}}^i{}_{A\tau} = \left(F^{-1}_{x\xi}F^i{}_A\right)_{,t} + \left[F^{-1}_{x\xi}\left(\hat{v}^j F^i{}_A - \hat{v}^i F^j{}_A\right)\right]_{,j} \tag{D.18}$$

The remaining components

$${}^{(3)}\tilde{\mathcal{C}}^t{}_{A\tau} = \mathcal{C}_A, \tag{D.19}$$

$${}^{(3)}\tilde{\mathcal{C}}^t{}_{AB} = 0 \tag{D.20}$$

are redundant. Note that everything is now expressed in terms of $F^i{}_A$ and $\hat{v}^i$, and we no longer need $\tilde{F}^a{}_A$.

The corresponding jump conditions are

$$\left[F^{-1}_{x\xi}F^n{}_A\right] = 0, \tag{D.21}$$

$$\left[\hat{F}^{-1}_{x\xi}(\hat{v}^n - s)\right] = 0, \tag{D.22}$$

$$\left[F^{-1}_{x\xi}F^n{}_{[A}F^{\|i}{}_{B]}\right] = 0, \tag{D.23}$$

$$\left[F^{-1}_{x\xi}F^{\|i}{}_A(\hat{v}^n - s)\right] - \left[F^{-1}_{x\xi}F^n{}_A\hat{v}^{\|i}\right] = 0, \tag{D.24}$$

where the n, $\|$ notation is as in Sec. 2.3. Note that these jump conditions are both more numerous and more complicated than the jump conditions (23,24) of the Eulerian framework.

Equivalence with the Eulerian framework Note that we have used $\mathcal{E}$ and $\mathcal{C}$ to denote the evolution equations and constraints in the mixed framework, and E and C for the Eulerian framework.

We have the following relations between the full and contracted equations for $F^i{}_A$,

$$\mathcal{C}_A = 2\psi^B{}_i\mathcal{C}^i{}_{AB}, \tag{D.25}$$

$$\mathcal{E} \quad = \frac{1}{2}\psi^B{}_i\left(\hat{v}^i\mathcal{C}_B - \mathcal{E}^i{}_B\right), \tag{D.26}$$

and the following relations between these equations and those for $\psi^A{}_i$:

$$\mathcal{E}^i{}_A = \delta_{ABC}\delta^{ijk}\left(\psi^C{}_l\hat{v}^l C^B{}_{jk} + \psi^C{}_j E^B{}_k\right), \tag{D.27}$$

$$\mathcal{C}^i{}_{AB} = \delta_{ABC}\delta^{ijk}C^C{}_{jk}. \tag{D.28}$$

As these relations between differential equations involve multiplication by one or more factors of ψ^A_i, which in general is not continuous, the corresponding jump conditions may be inequivalent. In particular, it is not clear if (D.22) follows from (D.24), if (D.21) follows from (D.23), if (D.23) is equivalent to (23) or if (D.24) is equivalent to (24). However, a detailed calculation shows that all these relations hold.

As an example of these calculations, consider

$$\begin{aligned}\left[F^{-1}_{x\xi}F^n{}_A\right] &= \left[\delta^{njk}\delta_{ABC}\psi^B{}_j\psi^C{}_k\right] \\ &= 2\delta^{nij}\delta_{ABC}\left[\psi^B{}_{\|i}\psi^C{}_{\|j}\right],\end{aligned} \tag{D.29}$$

where in the first equality we have used the cofactor rule and the assumption that F is the inverse of ψ, and in the second equality we have used that δ_{ABC} and δ^{ijk} are continuous. From (D.29) we see that (23) implies (D.21) (as claimed above), but the reverse is not true. In fact, the right-hand side of (D.29) vanishes if and only if

$$\left[\psi^A{}_{\|i}\right] = \alpha^A k_{\|i} \tag{D.30}$$

for some matter space vector α^A and spatial covector k_i. That is why the jump condition (D.23) also needs to be imposed.

In the papers [18, 17, 16, 32, 12, 13] only (D.22), (D.24) and (D.21) are explicitly given, but (D.23) appear to have been overlooked. In particular, the initial data for the second Riemann numerical test of [12] (BDRT2) and the initial data for the fifth Riemann numerical test of [13] (TRT5) explicitly violate (D.23). As noted in [28], not imposing the constraints (19), or equivalently (D.23), in full corresponds to performing surgery (of the type illustrated in the right panel of Fig. 1) at the discontinuity. Moreover, once the initial data violate the constraints, the subsequent evolution depends on how constraints have been added to the evolution equations.

Equations written in terms of the density We have already noted that with (30) and (38), (D.16) is just particle number conservation (37). Note that in weak solutions, we must demand that $\sqrt{k_\xi}$ is everywhere continuous, a property that is conserved under advection.

$F_{x\xi}$ can also be replaced by n in the other equations of the mixed framework. Defining

$$f^i{}_A := \frac{F^i{}_A}{\sqrt{k_\xi}}, \tag{D.31}$$

we can write (D.15) and (D.18) as

$$\left(W\sqrt{\gamma_\xi}\, n f^i{}_A\right)_{,i} = 0, \tag{D.32}$$

$$\left(W\sqrt{\gamma_\xi}\, n f^i{}_A\right)_{,t} + \left[W\sqrt{\gamma_\xi}\, n\left(f^i{}_A\hat{v}^j - f^j{}_A\hat{v}^i\right)\right]_{,j} = 0. \tag{D.33}$$

For fixed matter space index ${}_A$, these happen to be identical with the divergence constraint and the induction equation for the magnetic field in the formulation [31] of ideal magnetohydrodyamics (MHD) in general relativity.

Taking the Newtonian limit $W = 1$, γ_{ij} flat and assuming Cartesian coordinates so that $\sqrt{\gamma_x} = 1$, (37), (D.32) and (D.33) reduce to Eqs. (3.12), (3.26) and (3.22) of

[18], where $\sqrt{k_\xi}$ is called $\rho_{\rm ref}$. Further assuming $\sqrt{k_\xi} = 1$, they reduce to Eqs. (6), (9) and (1b) of [12] and Eqs. (3), (1) and (2) of [13].

In terms of ${f^i}_A$, the remaining equation, Eq. (D.17) can be written as

$$\left(\sqrt{k_\xi}\, W \sqrt{\gamma_\xi}\, n {f^i}_{[A} f^j_{B]}\right)_{,j} = 0, \tag{D.34}$$

where $\sqrt{k_\xi}$ reappears. As we have already noted, this constraint is not mentioned in [18, 12, 13, 17]. It also does not have an equivalent in MHD.

Appendix E. Discrete constraint preservation

The following class of conservative numerical schemes preserves a discrete version of the integrability constraints. With all other numerical variables defined as cell averages with, by convention, integer grid index values, define ${\psi^A}_i$ on relevant cell faces. To initialise them consistently, assign values to χ^A at cell centres at the initial time (in liquid as well as solid regions). Then initialize

$${\psi^A}_{x,i+1/2,j,k} = \frac{1}{\Delta x}\left(\chi^A_{i+1,j,k} - \chi^A_{i,j,k}\right), \tag{E.1}$$

$${\psi^A}_{y,i,j+1/2,k} = \frac{1}{\Delta y}\left(\chi^A_{i,j+1,k} - \chi^A_{i,j,k}\right), \tag{E.2}$$

$${\psi^A}_{z,i,j,k+1/2} = \frac{1}{\Delta z}\left(\chi^A_{i,j,k+1} - \chi^A_{i,j,k}\right). \tag{E.3}$$

The $\chi^A_{i,j,k}$ are used only for initialisation, and are not required afterwards. We then evolve using the conservative equations

$$\frac{d}{dt}{\psi^A}_{x,i+1/2,j,k} = \frac{1}{\Delta x}\left(\mathcal{F}^A_{i+1,j,k} - \mathcal{F}^A_{i,j,k}\right) \tag{E.4}$$

and similarly for ${\psi^A}_y$ and ${\psi^A}_z$, where the numerical flux $\mathcal{F}^A_{i,j,k}$ is some approximation to ${\psi^A}_j \hat{v}^j$ at cell centres, suitably limited to enforce the TVD property. Then a discrete version of ${\psi^A}_{x,y} - {\psi^A}_{y,x} = 0$, evaluated at relevant cell edges:

$$\begin{aligned}&\frac{1}{\Delta y}({\psi^A}_{x,i+1/2,j+1,k} - {\psi^A}_{x,i+1/2,j,k})\\ &-\frac{1}{\Delta x}({\psi^A}_{y,i+1,j+1/2,k} - {\psi^A}_{y,i,j+1/2,k}) = 0,\end{aligned} \tag{E.5}$$

and similarly for the other two commutators, is obeyed at all times if it is obeyed initially. The fundamental idea is that the numerical fluxes $\mathcal{F}^A$ are a representation of the time derivatives of the underlying χ^A, and hence are the same for the update of ${\psi^A}_x$, ${\psi^A}_y$ and ${\psi^A}_z$. The discrete constraints act as discrete integrability conditions that allow us to reconstruct the $\chi^A_{i,j,k}$ by summation if desired.

Appendix F. Riemann tests on a 2-dimensional grid

As a first test of the role of the constraints in hyperbolicity, we numerically solve Riemann problems on a 2-dimensional grid, with the initial discontinuity at an angle to the grid. Assume the grid consists of $n_x \times n_y$ cells, surrounded by the necessary number of ghost cells. After each time update, the ghost points are filled using periodic boundary conditions, identifying cell (i, j) with $(i + n_x, j)$ in the x direction, but (i, j) with $(i + \delta_x, j + n_y)$ in the y direction, where δ_x is an offset. Consistently with these

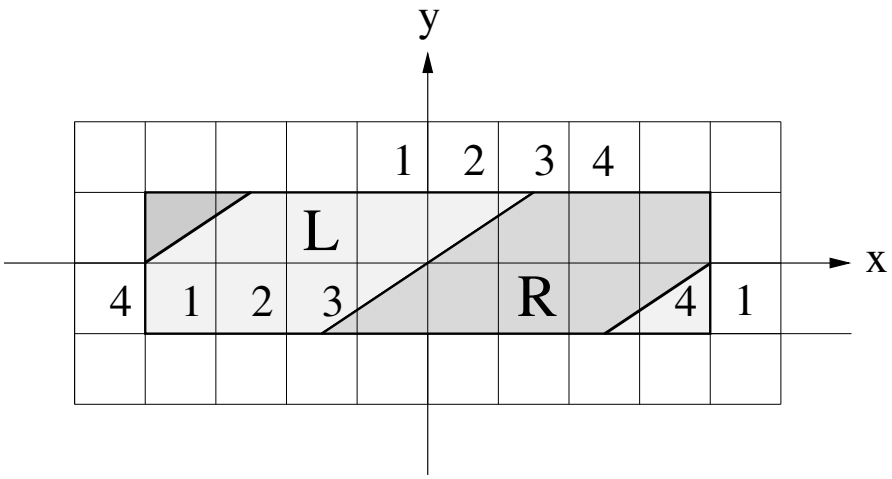

Figure F1: Example of a two-dimensional grid with shifted periodic boundary conditions, with $n_x = 8$, $n_y = 2$ and $\delta_x = 3$. The physical grid is surrounded by one ghost cell on each side. In reality, n_x would be much larger, while n_y ranges from 1 to a few, and δ_x from 0 to a few, with no common factor. The placement of the left and right state of a Riemann problem is shown by the letters L and R and shading. Cells are initialised with the left or right state depending on the position of the cell *center*. The numbers 1, 2, 3, 4 identify four physical cells and the ghost cells they donate values to. The initial discontinuity is at an angle α from the y axis, with $\tan\alpha = \delta_x/n_y$ ($= 3/2$ in this example), and goes through the point $x = y = 0$.

boundary conditions, the initial discontinuity is then placed on a line of $x/y = \delta_x/n_y$ (assuming that the grid spacing is the same in the x and y directions). This is illustrated in Fig. F1.

As the x and y directions are interchangeable, the slope δ_x/n_y and its inverse pose the same Riemann test. (Less obviously, in our implementation those two tests also have roughly equal computational cost.) We choose $n_y \geq \delta_x$ (and typically $\delta_x = 1$) so that the initial discontinuity is always closer to the y axis (where it is in the 1D tests), and use the x axis as an approximation to a line normal to the initial discontinuity when taking a cut through the solution.

Appendix G. A two-dimensional cylindrical grid

Source terms One important difference when moving from Cartesian to cylindrical coordinates is that the source terms for the equations of motion derived from the stress-energy tensor become non-zero. When the cylindrical Minkowski metric, $\mathrm{diag}(-1, r^2, 1, 1)$, is used, we find that the only non-zero source term is

$$\mathcal{S}(S_r) = r^2 T^{\theta\theta}. \tag{G.1}$$

Transforming initial data and output We start by setting the initial data using Cartesian coordinates; we then transform both the matter-space and spacetime

coordinates to cylindrical coordinates. We use the Jacobian matrix

$$\frac{\partial x^{a'}}{\partial x^b} = \begin{pmatrix} \frac{x}{r} & \frac{y}{r} & 0 \\ -\frac{y}{r^2} & \frac{x}{r^2} & 0 \\ 0 & 0 & 1 \end{pmatrix}, \tag{G.2}$$

and its inverse to transform covariant and contravariant spatial indices, where $x^{a'} = (r, \theta, z)$ and $x^b = (x, y, z)$, and the usual transformation between (x, y) and (r, θ) is used:

$$x = r\cos\theta, \quad y = r\sin\theta. \tag{G.3}$$

The same transformation applies to the matter space indices, with $\xi^{A'} = (R, \Theta, Z)$ and $\xi^A = (X, Y, Z)$ in place of $x^{a'}$ and x^b. To do this for the initial data, we find the matter-space coordinates in terms of the spacetime coordinates by integrating ${\psi^A}_i$, which is, by definition, ${\psi^A}_i = \partial\xi^A/\partial x^i$. Where the initial data for ${\psi^A}_i$ is piecewise constant, as is the case for all our tests here, this integration just gives

$$\xi^A = {\psi^A}_i x^i + \text{const}, \tag{G.4}$$

with the constants chosen so that the ξ^A are continuous at the initial discontinuity. In order to compare the results in cylindrical coordinates with those in Cartesian coordinates, we need to transform v^i and ${\psi^A}_i$ between the two coordinate systems at later times. For this diagnostic purpose (only), we advect the (Cartesian) matter coordinates $\xi^A(x^i, t)$ with the fluid. $\xi^{A'}$ and ξ^A are then always linked by the standard formula (G.3).

Limitations on the initial data In these tests, we have hidden the planar or axisymmetry by making the problem appear to depend nontrivially on two coordinates (r, θ). However, we do not want to hide the z-translation symmetry in order to keep simulations two-dimensional. Now, if the Cartesian components, ${\psi^A}_z$, were non-zero, then the matter-space coordinates, ξ^A, would be dependent on z, making the transformation, as well as the cylindrical components of ${\psi^A}_i$, z-dependent.

To avoid these problems, we use only tests with ${\psi^A}_z = 0$ when we are using cylindrical coodinates. Because we wanted to compare to published results, we use a version of BDRT1 [12] which differs from the original by a linear transformation of the matter space coordinates (and so changes ${\psi^A}_i$), and transform the results back to the original coordinates for the purpose of comparison. The initial data for this test is described in Appendix K.

Boundaries We have used simple copy boundary conditions in the r direction, and periodic boundaries in the θ direction, while ensuring that the computational grid extends over a range of 2π in θ. The copy boundaries are not correct in general; these incorrect boundary conditions are what cause the visible problems near the boundaries in the BDRT1 test on the cylindrical grid, visible in Fig. 13b. Since we do not anticipate using cylindrical coordinates (or spherical coordinates) in the future, we use copy boundary conditions for simplicity's sake, and note where the incorrect boundary conditions have caused problems.

Appendix H. Shear invariants and "the" shear scalar

The three eigenvalues of $\eta^A{}_B$ can be parameterised as $\{a, b, 1/(ab)\}$. We then find that in the unsheared state $a = b = 1$,

$$I^1 = I^2 = 3, \tag{H.1}$$

$$I^1_{,a} = I^1_{,b} = I^2_{,a} = I^2_{,b} = 0, \tag{H.2}$$

$$I^1_{,aa} = I^1_{,bb} = 2, \quad I^1_{,ab} = 1, \tag{H.3}$$

$$I^2_{,aa} = I^2_{,bb} = 8, \quad I^2_{,ab} = 4. \tag{H.4}$$

Hence $4(I^1 - 3)$ and $I^2 - 3$ are the same function of the shear up to quadratic order. This is not the result of a bad choice of I^α but a property of any shear invariant. It is related to the fact that the characteristic speeds in the unsheared state depend on f_1 and f_2 only through the one combination $f_1 + 4f_2$ that appears in the shear modulus (167).

Therefore, to model linear elasticity correctly, it is sufficiently general to make the ansatz

$$\epsilon(s, n, I^\alpha) = \check{\epsilon}(n, s) + \frac{\check{\mu}(n, s)}{n}\mathcal{S}(I^1, I^2), \tag{H.5}$$

where the single *shear scalar* $\mathcal{S}$ obeys

$$\mathcal{S} = 0, \tag{H.6}$$

$$2\frac{\partial \mathcal{S}}{\partial I^1} + 8\frac{\partial \mathcal{S}}{\partial I^2} = 1 \tag{H.7}$$

in the unsheared state $I^1 = I^2 = 3$, but is otherwise arbitrary. For any such choice of $\mathcal{S}$, $\check{\mu}(n, s)$ evaluates to the usual shear modulus (167) in the Newtonian limit, and the equations of motion are the same when linearised about the unsheared state.

Clearly there are many possibilities of defining a shear scalar that obeys these conditions, but we are not aware of any physical reason given in the literature for why a specific choice should be preferred, or of values given for f_1 and f_2 independently. Indeed, different choices can only be distinguished in a nonlinear deformation regime, in which case there is no particular reason to assume that ϵ does not depend on I^1 and I^2 in a more generic way.

An equation of state for copper used in [13] uses the shear scalar

$$\mathcal{S}_{\text{Cran}} := \frac{3I^2 - (I^1)^2}{12}, \tag{H.8}$$

which is quadratic in the eigenvalues of $\eta^A{}_B$. In [9] the shear scalar

$$\mathcal{S}_{\text{KS}} := \frac{(I^1)^3 - I^1 I^2 - 18}{24}, \tag{H.9}$$

which is cubic, is suggested for what seem to be aesthetic reasons. Yet another shear scalar is

$$\mathcal{S}_{\text{VM}} := s^{ab}s_{ab} = \frac{I^2 - 2I^1 + 3}{4}, \tag{H.10}$$

where

$$s_{ab} := \frac{1}{2}(h_{ab} - \eta_{ab}) \tag{H.11}$$

is the "constant volume shear tensor" defined in [8]. In the Newtonian limit, near the unsheared state, $\mathcal{S}_{\text{VM}}$ is related to the Von Mises stress scalar (assuming stress and strain are related linearly). It gives the same values of f_1 and f_2 in the unsheared state as $\mathcal{S}_{\text{Cran}}$.

Appendix I. Equations of state

We now consider examples of equations of state of the form (H.5). The following general expressions will be useful:

$$h = 1 + \check{\epsilon} + \frac{\check{\mu}}{n}\mathcal{S} + \frac{p}{n}, \tag{I.1}$$

$$p = n^2 \frac{\partial \check{\epsilon}}{\partial n} + \left(n \frac{\partial \check{\mu}}{\partial n} - \check{\mu} \right) \mathcal{S}, \tag{I.2}$$

$$f_\alpha = \frac{\check{\mu}(n,s)}{n} \frac{\partial \mathcal{S}}{\partial I^\alpha}. \tag{I.3}$$

In principle we can eliminate s from these two equations to obtain p, f_1 and f_2, as functions of (n, h, I^1, I^2), which we need in the recovery of the primitive from the conserved variables.

A toy relativistic EOS As a toy model for a relativistic equation of state, we take $\check{\epsilon}$ from the commonly used "Gamma-law" hot equation of state, and make the shear modulus $\check{\mu}$ a power of the density only, namely

$$\check{\epsilon}(n,s) = \frac{K(s)}{\Gamma - 1} n^{\Gamma - 1}, \tag{I.4}$$

$$\check{\mu}(n,s) = \kappa n^\lambda, \tag{I.5}$$

where Γ, κ and λ are constants. This is motivated by the fact that in neutron star crusts $\mu \propto n^{4/3}$, with the factor of proportionality only weakly temperature-dependent. The bulk modulus in neutron stars is given by the nuclear interactions, while the shear modulus is provided by Coulomb interactions, which makes it independent and much smaller. Following [9], we choose $\mathcal{S}$ as $\mathcal{S}_{\rm KS}$ given by (H.9).

The expressions we need for the conserved to primitive variables conversion are then

$$p(h, n, I^\alpha) = \frac{\Gamma - 1}{\Gamma} n(h-1) + \frac{\lambda - \Gamma}{\Gamma} \kappa n^\lambda \mathcal{S}, \tag{I.6}$$

$$p(\epsilon, n, I^\alpha) = (\Gamma - 1) n\epsilon + (\lambda - \Gamma)\kappa n^\lambda \mathcal{S}, \tag{I.7}$$

$$h(p, n, I^\alpha) = 1 + \frac{\Gamma}{\Gamma - 1}\frac{p}{n} + \frac{\Gamma - \lambda}{\Gamma - 1}\kappa n^{\lambda - 1}\mathcal{S}, \tag{I.8}$$

$$f_1 = \kappa n^{\lambda - 1} \frac{3(I^1)^2 - I^2}{24}, \tag{I.9}$$

$$f_2 = -\kappa n^{\lambda - 1} \frac{I^1}{24}. \tag{I.10}$$

The characteristic speeds in the unsheared state are

$$\lambda_T^2 = \frac{\kappa n^{\lambda - 1}}{1 + \Gamma\epsilon}, \tag{I.11}$$

$$\lambda_L^2 = \frac{\Gamma(\Gamma - 1)\epsilon + \frac{4}{3}\kappa n^{\lambda - 1}}{1 + \Gamma\epsilon}. \tag{I.12}$$

Cranfield EOS The equation of state for copper used in [13] for Newtonian shock tube problems, translated into our notation, is

$$\epsilon(s, n, I^\alpha) = A(n) + B(n)K(s) + C(n)\mathcal{S}, \tag{I.13}$$

$$A := \frac{K_0}{2\alpha^2}\left[\left(\frac{n}{n_0}\right)^{\alpha} - 1\right]^2, \tag{I.14}$$

$$B := c_V T_0 \left(\frac{n}{n_0}\right)^{\gamma}, \tag{I.15}$$

$$K := e^{\frac{s}{c_V}} - 1, \tag{I.16}$$

$$C := B_0 \left(\frac{n}{n_0}\right)^{\beta+4/3}, \tag{I.17}$$

where $\mathcal{S}$ is $\mathcal{S}_{\rm Cran}$ given by (H.8). We need the following forms of the equation of state:

$$p(s, n, I^\alpha) = n\left[nA' + \gamma BK + (\beta + 4/3)C\mathcal{S}\right], \tag{I.18}$$

$$p(h, n, I^\alpha) = \frac{n}{\gamma+1}\Big[\gamma(h-1) - \gamma A + nA' + (\beta + 4/3 - \gamma)C\mathcal{S}\Big], \tag{I.19}$$

$$p(\epsilon, n, I^\alpha) = n\Big[\gamma\epsilon - \gamma A + nA' + (\beta + 4/3 - \gamma)C\mathcal{S}\Big], \tag{I.20}$$

$$h(p, n, I^\alpha) = 1 + \frac{\gamma+1}{\gamma}\frac{p}{n} + A - \frac{1}{\gamma}nA' - \frac{1}{\gamma}(\beta + 4/3 - \gamma)C\mathcal{S}, \tag{I.21}$$

$$f_1 = -\frac{CI^1}{6}, \tag{I.22}$$

$$f_2 = \frac{C}{4} \tag{I.23}$$

Appendix J. Constructing exact solutions

The exact solution of the Riemann problem is a standard test for HRSC methods. For Newtonian elasticity exact solvers have been constructed both by Miller [28] and by Barton et al. [12]. In the relativistic case here we have not constructed a generic solver to compute the full Riemann problem solution. As noted by [12], this can be extremely sensitive to initial guesses used. Instead we construct exact solutions by specifying the wave structure explicitly in advance and solving across each wave.

As summarized in [12], with piecewise constant initial data the generic solution will contain seven self-similar waves. The central wave will be a contact discontinuity, and the other waves will be genuinely nonlinear. We assume that the solutions are simple shocks or rarefactions. We then solve across each wave in the following manner.

Shock wave We assume that the primitive variables to the left of the wave, $\mathbf{w}_L$, are given. We then impose the value *either* of the shock speed $s^{(p)}$ or of one component of the variables to the right of the wave, $\mathbf{w}_R$. The Rankine-Hugoniot conditions

$$\mathbf{f}(\mathbf{w}_R) - \mathbf{f}(\mathbf{w}_L) = s^{(p)}\left[\mathbf{q}(\mathbf{w}_R) - \mathbf{q}(\mathbf{w}_L)\right] \tag{J.1}$$

then form a system of nonlinear equations for the remaining components of $\mathbf{w}_R$ and, where necessary, for the shock speed $s^{(p)}$. Here $^{(p)}$ denotes the wave number counting from the left.

This problem is solved explicitly using the Matlab solver `fsolve`. It is usually necessary to experiment with the imposed value and initial guesses in order to construct a solution satisfying the Lax entropy condition

$$\lambda^{(p)}(\mathbf{w}_L) > s^{(p)} > \lambda^{(p)}(\mathbf{w}_R). \tag{J.2}$$

The construction of the eigenvalues $\lambda^{(p)}$ is discussed below.

Contact discontinuity A contact must satisfy the Rankine-Hugoniot conditions (J.1) combined with the restriction that the wave speed s matches the normal velocity on either side of the wave. Hence we can use the same techniques as for the shock with the value of the velocity imposed.

Rarefaction wave As noted by [12] the solution across a rarefaction wave is given by

$$\frac{\partial \mathbf{w}}{\partial \xi} = \frac{\mathbf{r}^{(p)}(\mathbf{w})}{\mathbf{r}^{(p)}(\mathbf{w}) \cdot \nabla_{\mathbf{w}} \lambda^{(p)}(\mathbf{w})}. \tag{J.3}$$

Here $\xi = x/t$ is the self-similarity variable. We have that $\lambda^{(p)}(\mathbf{w}_L) \leq \xi$ where $^{(p)}$ labels the wave number and $\mathbf{w}_L$ is given, as above. We impose that $\xi \leq \xi_R = \lambda^{(p)}(\mathbf{w}_R)$ to stop the integration. In addition $\mathbf{r}^{(p)}$ are the right eigenvectors associated with the p^{th} eigenvalue $\lambda^{(p)}$, and $\nabla_{\mathbf{w}}$ denotes the gradient operator with respect to the vector of primitive variables.

All characteristic information $(\lambda^{(p)}, \mathbf{r}^{(p)})$ is constructed from the Jacobian matrix

$$J = \frac{\partial \mathbf{f}(\mathbf{w})}{\partial \mathbf{q}(\mathbf{w})} = (\nabla_{\mathbf{w}} \mathbf{q})^{-1} \nabla_{\mathbf{w}} \mathbf{f}. \tag{J.4}$$

As in the Newtonian case discussed in [12] we need to explicitly modify the calculated Jacobian to build in the hyperbolicity corrections as in equation (17).

Given an explicit left state $\mathbf{w}_L$ the numerical solution is found by solving the ODE (J.3) for $\mathbf{w}$ with initial data $\mathbf{w}_L$ in $\lambda^{(p)}(\mathbf{w}_L) \leq \xi \leq \xi_R$. Explicitly we use the `ode45` routine with Matlab. The Jacobian J is constructed using explicit finite differencing by varying each component of $\mathbf{w}$ by a small value h. Standard Matlab routines were used to construct and sort the characteristic information. The gradient $\nabla_{\mathbf{w}} \lambda^{(p)}(\mathbf{w})$ was also constructed using explicit finite differencing. In all cases 6^{th} order finite differencing combined with Richardson extrapolation was used to ensure sufficient accuracy.

There are two potential problems with this construction. First, as noted by [12], we have no guarantee that equation (J.3) has a unique solution. This would imply that the true solution is a compound wave, and breaks the assumptions made here. Second, the numerical construction of the characteristic information is extremely sensitive when the eigenvalues are close to each other. This appears to be the case for the problems and equations of state considered below, and means that for the slower 3 and 5 waves next to the contact we are forced to construct very small rarefaction fans.

In principle there is no reason why the procedure above could not be extended to construct a full Riemann solver. However, such a solver would have little practical utility, even if it could be made generic and robust. Numerical experiments have shown that it is faster to compute an approximate solution using 800 grid cells than it is to construct *one* exact solution with a pre-specified wave structure. Even allowing for the massive speed improvements possible within our current exact solver, it is clearly impractical for use within an evolution code.

Appendix K. Initial data for numerical tests

We used several sets of initial data that were defined in published papers; this was done to ensure that our code agreed with Newtonian results produced previously [12] [13]. Because both papers chose entropy, s, as a primitive variable, instead of the pressure, p, we list the initial entropy value here, and calculate the pressure from the entropy when the system is initialized.

For the following sets of initial data, the spacetime metric is the Minkowski metric, and the matter-space metric is the Euclidean metric in Euclidean coordinates normalized with the initial density of the elastic medium, n_0; we note that while we must convert units of velocity to geometrized units, we do not need to convert units of density or of length, as long as we are consistent throughout the code. For this paper the value $n_0 = 8.93$ g/cm^3 was used for the BDRT tests (from [12]) and $n_0 = 8.9$ g/cm^3 was used for the TRT tests (from [13]). In addition to this, for each of these situations, the Cranfield equation of state, described in Appendix I, was used. For comparison purposes, the velocities in this section are taken to be in km s^{-1}, while the entropy is in kJ g^{-1}K^{-1}.

BDRT1 This is the same as *Testcase 1* in [12]. It allows us to examine the entire seven-wave structure of the solution. Using the Cranfield EOS above, the solution consists of three left-travelling rarefaction waves, a right-travelling contact, two right-travelling rarefactions, and a right-travelling shock wave. The initial data is presented for the state vector $\mathbf{w} = (v^i, F^i{}_A, s)$ in the mixed framework given in Appendix D, and all other quantities are derived from them:

$$\begin{aligned}
\mathbf{w}_L &= \left\{ \begin{pmatrix} 0 \\ 0.5 \\ 1 \end{pmatrix}, \begin{pmatrix} 0.98 & 0 & 0 \\ 0.02 & 1 & 0.1 \\ 0 & 0 & 1 \end{pmatrix}, 0.001 \right\}, \\
\mathbf{w}_R &= \left\{ \begin{pmatrix} 0 \\ 0 \\ 0 \end{pmatrix}, \begin{pmatrix} 1 & 0 & 0 \\ 0 & 1 & 0.1 \\ 0 & 0 & 1 \end{pmatrix}, 0 \right\}.
\end{aligned} \tag{K.1}$$

BDRT1 Transformed As explained in Appendix G, we cannot directly use the original BDRT1 test with the cylindrical grid. To remedy this, we obtain a transformed version of the BDRT1 test presented in [12] by transforming the lower matter-space indices as $F^i{}_{A'} = F^i{}_B \Lambda^B{}_{A'}$ where

$$\Lambda^B{}_{A'} := \frac{\partial \xi^B}{\partial \xi^{A'}} = \begin{pmatrix} 1 & 0 & 0 \\ 0 & 1 & -0.1 \\ 0 & 0 & 1 \end{pmatrix}, \tag{K.2}$$

and the upper matter-space indices using its inverse. The transformed version is as follows:

$$\begin{aligned}
\mathbf{w}_L &= \left\{ \begin{pmatrix} 0 \\ 0.5 \\ 1 \end{pmatrix}, \begin{pmatrix} 0.98 & 0 & 0 \\ 0.02 & 1 & 0 \\ 0 & 0 & 1 \end{pmatrix}, 0.001 \right\}, \\
\mathbf{w}_R &= \left\{ \begin{pmatrix} 0 \\ 0 \\ 0 \end{pmatrix}, \begin{pmatrix} 1 & 0 & 0 \\ 0 & 1 & 0 \\ 0 & 0 & 1 \end{pmatrix}, 0 \right\},
\end{aligned} \tag{K.3}$$

where the matter-space metric is also transformed so that, over the whole computational domain, it is

$$k_{AB} = \begin{pmatrix} n_0^{2/3} & 0 & 0 \\ 0 & n_0^{2/3} & -0.1 n_0^{2/3} \\ 0 & -0.1 n_0^{2/3} & n_0^{2/3} \end{pmatrix}. \tag{K.4}$$

4-wave relativistic solution We constructed a range of relativistic solutions, mostly consisting of a single shock or rarefaction, using the technique outlined in Appendix J. The toy relativistic equation of state given above is used, with parameters $\Gamma = 5/3$, $\lambda = 4/3$, and $\kappa = 1/2$. In particular, we present a solution with four nonlinear waves. The two left-going waves (1- and 2-waves) are rarefactions. The contact is trivial, as are the central (3- and 5-waves) nonlinear waves. The slower right-going wave (a 6-wave) is a rarefaction, and the fast right-going 7-wave is a shock. The initial data is presented for the state vector $\mathbf{w} = (v^i, \psi^A{}_i, p)$, truncated to 6 significant figures, and all other quantities are derived from them:

$$\mathbf{w}_L = \left\{ \begin{pmatrix} 0.05 \\ 0.1 \\ 0.2 \end{pmatrix}, \begin{pmatrix} 1.5 & 0 & 0 \\ -0.5 & 1 & 0 \\ 0.5 & 0 & 1 \end{pmatrix}, 1.86054 \right\}, \tag{K.5}$$

$$\mathbf{w}_R = \left\{ \begin{pmatrix} 0.469381 \\ -0.0332532 \\ 0.349709 \end{pmatrix}, \begin{pmatrix} 0.764910 & 0 & 0 \\ -0.541672 & 1 & 0 \\ 0.369075 & 0 & 1 \end{pmatrix}, 0.450123 \right\} \tag{K.6}$$

Rotor tests In addition to Riemann problem style tests we consider a genuinely two-dimensional rotor test. The Newtonian rotor test was suggested by [33], where the evolution was shown using a high-order finite element technique. The domain is cylindrical, of total radius 0.5. The material is initially at rest except in the rotor, represented by a cylinder of radius 0.1, within which it rotates with angular velocity $\omega = 10$. The material is not deformed (i.e., $F^i{}_A$ is the unit matrix) nor hot (i.e., $s = 0$). All other matter properties follow the Riemann tests above. That is, the initial density is given by $n_0 = 8.93\ \mathrm{g/cm^3}$ and the Cranfield equation of state, described in Appendix I, was used. Here, as we have used a Cartesian grid, we have simulated the full domain $x, y \in [-0.5, 0.5]$.

We have developed a new ring rotor version of the Dumbser Rotor from [33] so that, while using two-dimensional cylindrical coordinates, we do not have to include the axis of the coordinate system. The inner and outer areas of the grid have the same initial data, while the central region of the grid differs from these states only in that it has a non-zero velocity. Aside from the velocity, the initial data for this test is exactly the same as for the Dumbser Rotor; the velocity in the inner and outer regions is 0, while the central region has a uniform angular velocity of $\omega = 1.0$.

We suggest a relativistic rotor test as a direct comparison with the Newtonian version. The domain remains the same as the Newtonian case. The angular velocity is reduced to $\omega = 0.5$. The material is initially set so that $\psi^A{}_i$ is the unit matrix and $p = 1$. As the shear also depends on the velocity through $\psi^A{}_t$, the material is sheared within the rotor initially, in contrast to the Newtonian case, but this is small. As in the Riemann tests above we use the toy relativistic equation of state given in Appendix I, with parameters $\Gamma = 5/3$, $\lambda = 4/3$, and $\kappa = 1/2$.

References

[1] N. Chamel and P. Haensel, Living Rev. in Relativity, **2008**-10 (2008).
[2] M. A. Alpar, H. F. Chau, K. S. Cheng, and D. Pines, Astrophys. J. **459**, 706 (1996).
[3] R. C. Duncan, Astrophys. J. **498**, L45 (1998).
[4] L. Samuelsson and N. A. Andersson, MNRAS **374**, 256 (2007).
[5] M. Gabler, P. Cérda-Durán, J. A. Font, E. Müller and N. Stergioulas, MNRAS **410**, L37 (2011).
[6] C. Horowitz and K. Kadau, Phys. Rev. Lett. **102**, 191102 (2009).
[7] L. Baiotti, B. Giacomazzo and L. Rezzolla, Phys. Rev. D **78**, 084033 (2008).
[8] B. Carter and H. Quintana, Proc. Roy. Soc. Lond. A **331**, 57 (1972).
[9] M. Karlovini and L. Samuelsson, Class. Quant. Grav. **20**, 3613 (2003); M. Karlovini and L. Samuelsson, Class. Quant. Grav. **22**, 771 (2005).
[10] R. Beig and B. G. Schmidt, Class. Quant. Grav. **20**, 889 (2003).
[11] J. A. Font, Living Rev. in Relativity, **2008**-7 (2008).
[12] P. T. Barton, D. Drikakis, E. Romenski and V. A. Titarev, J. Comp. Phys. **228**, 7046 (2009).
[13] V. A. Titarev, E. Romenski and E. F. Toro, Int. J. Numer. Meth. Eng. **73**, 897 (2008).
[14] G. H. Miller and P. Colella, J. Comp. Phys. **167**, 131 (2001).
[15] J. A. Trangenstein and P. Colella, Comm. Pure Appl. Math. **44**, 41 (1991).
[16] S. K. Godunov and E. I. Romenski, J. Appl. Mech. and Technical Phys. **13**, 868 (1972).
[17] S. K. Godunov and I. M. Peshkov, Comp. Math. and Math. Phys. **48**, 975 (2008).
[18] B. J. Plohr and D. H. Sharp, Adv. Appl. Math. **9**, 481 (1988).
[19] M. Wernig-Pichler, PhD thesis, 2006, arXiv:gr-qc/0605025.
[20] C. Gundlach and J. M. Martín-García, Class. Quant. Grav. **23**, S387 (2006).
[21] G. H. Miller and P. Colella, J. Comp. Phys. **183**, 25 (2002).
[22] S. Millmore and I. Hawke, Class. Quantum Grav. **27**, 015007 (2010).
[23] B. J. van Leer, Lecture Notes in Physics **18**, 163 (1973).
[24] B. Einfeldt, SIAM Journal on Numerical Analysis **25**, 294 (1988).
[25] Exact solution obtained from P. Barton as a private communication.
[26] W. Noh, J. Comp. Phys. **72**, 78 (1987).
[27] J. M. Martí and E. Müller, Living Rev. in Relativity, **2003**-7 (2003).
[28] G. H. Miller, J. Comp. Phys. **193**, 198 (2004).
[29] R. Beig, Lect. Notes Phys. **692**, 101 (2006).
[30] A. M. Anile, *Relativistic fluids and magneto-fluids : with applications in astrophysics and plasma physics*, Cambridge University Press, 1989.
[31] L. Anton et al, Astrophys. J. **637**, 296 (2006).
[32] X. Garaizar, J. Elasticity **26**, 43 (1991).
[33] M. Dumbser, D. Balsara, E. Toro and C. D. Munz, J. Comp. Phys. **227**, 8209 (2008).